Journal of Materials Chemistry A

ROYAL SOCIETY OF CHEMISTRY

REVIEW

View Article Online
View Journal | View Issue

Cite this: J. Mater. Chem. A, 2024, 12, 22372

Polymer-based films for all-in-one piezo-driven self-charging power systems

Kewei Shu, *[a] Wenjuan Li,[a] Qijie Wu,*[b] Yan Zong,[c] Chen Zhao,[d] Yi Zhang[a] and Caiyun Wang *[e]

The evolution of wearable and implantable electronics has been rapidly advancing alongside the emergence of smart technologies. This raises additional requirements on the energy storage system for powering these devices. Self-chargeability is a highly demanded feature that can prolong the service life without the need for an external power supply. The ubiquitous mechanical energy makes it an ideal source for charging an energy storage system by utilizing the piezoelectric effect. Therefore, the incorporation of an energy harvesting component into an energy storage unit to form a highly integrated all-in-one piezo-driven self-charging power system (SCPS) has been attracting extensive attention. Piezoelectric polymer-based films are the key components in SCPSs either as separators or electrolytes, which determine the self-charging performance of the device. This review aims to provide an overview of recent advances in the application of polymer-based films in SCPSs. The configuration and working mechanism of piezo-driven SCPSs are introduced, and key materials used for polymer-based piezoelectric films are summarized. The discussion on latest developments in polymer-based piezoelectric components focuses on materials design and self-charging performance. The future directions and new perspectives for the development of polymer piezoelectric films for SCPSs are also presented. This work may provide guidelines and useful information for practical implementation of SCPSs in wearable and implantable electronics.

Received 29th April 2024
Accepted 14th July 2024

DOI: 10.1039/d4ta02965h

rsc.li/materials-a

1. Introduction

Wearable electronics and implantable devices have evolved rapidly over the past two decades, particularly with the advent of smart and internet of things (IoT) based technologies.[1–4] The development of these devices is hindered by the constraints of traditional rigid energy storage systems. In response, a flexible energy storage device that is able to function normally during mechanical deformation is designed to meet the requirement of flexibility.[5,6] However, they are still inconvenient for wearable electronics, especially implantable devices, due to their limited lifetime and the frustrating replacement or recharging process. It is highly desirable for wearable and implantable devices to harvest energy from ambient sources such as solar, heat, vibrations, and motions.[7–11] Biomedical implants and wearable electronics require relatively low power consumption and high environmental adaptability. They frequently encounter mechanical deformations such as breathing, arm-motions and heart pulses. Once these energies are collected and efficiently utilized, they may partially or even fully compensate for the energy consumption of these electronics. In the working scenario of wearable and implantable devices, piezoelectric nanogenerators (PENGs) stand out as highly attractive energy harvesting technology. They are capable of converting low-frequency mechanical energy (vibration, pressure, and body motion) into electric energy, making them ideal for integration with the above-mentioned wearable devices.[12–16]

However, there are still some issues to be addressed if wearable devices were to be directly powered by PENGs. The application scenario of such devices would be restricted due to asynchrony of distributed, time-variable mechanical energy and power requirements. In such circumstances, it holds great promise to save and accumulate the fluctuating, small amount of piezo-energy using energy storage devices to ensure a stable power output. Nevertheless, the incorporation of energy harvesters into energy storage systems offers a more efficient way to offset the power consumption or even fully recharge the device. The concept of an integrated "self-charging" system is

[a]Xi'an Key Laboratory of Advanced Performance Materials and Polymers, School of Chemistry and Chemical Engineering, Shaanxi University of Science and Technology, Xi'an 710021, Shaanxi, China. E-mail: shukw@sust.edu.cn
[b]Institute of Quantum and Sustainable Technology (IQST), Department of Chemistry and Chemical Engineering, Jiangsu University, Zhenjiang 212013, Jiangsu, China. E-mail: qw988@ujs.edu.cn
[c]College of Bioresources Chemical and Materials Engineering, Shaanxi University of Science and Technology, Xi'an 710021, Shaanxi, China
[d]School of Materials and Energy, Guangdong University of Technology, Guangzhou 510006, China
[e]Intelligent Polymer Research Institute, Faculty of Engineering and Information Sciences, Innovation Campus, University of Wollongong, Wollongong, NSW 2500, Australia. E-mail: caiyun@uow.edu.au

then proposed which combines an energy harvester with an energy storage unit together and then has experienced considerable development.[17–21] At present, the dominant electrochemical energy storage (EES) systems consist of metal-ion batteries and supercapacitors. Rechargeable metal-ion batteries offer large energy, but they often necessitate long re-charging time. Nonetheless, the current secondary batteries exhibit a minimal memory effect and low self-discharge rate, which facilitate energy accumulation by the harvesting unit. Supercapacitors possess high power density and can deliver high instantaneous current output. However, they have low energy density. The combination of supercapacitors and energy harvesters facilitates "self-charging" and provides adequate power for wearable and implantable electronics.[22] Although a "joint" device can be easily fabricated by linking a PENG with a separated energy storage unit *via* an external circuit, a single and highly integrated all-in-one device that combines the energy harvester and energy storage unit together is preferred.[18] In the all-in-one type, one component serves multiple functions as both a piezoelectric nanogenerator and battery/supercapacitor component. The all-in-one piezo-driven self-charging power system (SCPS) is attracting the attention of researchers[20,22] and is also the focus of this review. It offers notable merits, such as simple configuration, high integration and versatility. This system is particularly well-suited for IoT-based wearable healthcare devices. The frequently encountered mechanical forces enable cumulative energy compensation for these low-power electronics, thereby providing prolonged device life (Fig. 1).[20]

There have been several excellent review papers about self-charging energy storage systems in the past five years. Some focused on providing an overview of all types of self-charging devices driven by various power sources such as solar cells, thermoelectrics, nanogenerators, *etc.*[20,21] Other reviews concentrated on the principle, mechanism, and utilization of materials for self-charging supercapacitors.[22,27,28] This review specifically focuses on summarizing the recent progress in polymer and polymer composite components in an all-in-one piezoelectric-driven SCPS including batteries and supercapacitors for flexible and wearable electronics. These polymer or polymer composite-based piezoelectric films are essential components that determine the self-charging ability of SCPSs. They serve as electrolytes and/or separators in the energy storage unit. As such, SCPSs can be regarded as a derivative of flexible PENGs. Therefore, the pursuit of polymer-based separators or solid-state electrolyte with high intrinsic piezoelectricity is the simplest and most efficient way to realize efficient piezo-driven self-charging. Given their extensive application in battery separators and intrinsic modulable piezoelectric effect, PVDF and its co-polymers have become the first and most extensively studied polymer piezo-separators.[29,30] The piezoelectric properties of PVDF can be enhanced *via* structure engineering, processing techniques, and incorporation of inorganic piezoelectric fillers.[31,32] These piezoelectric electrolytes can be prepared either by using PVDF as a polymer matrix or by combing a non-piezoelectric polymer with piezoelectric fillers, as in flexible PENGs based on non-piezoelectric polymers. Additionally, the unique feature of the piezo-ionic effect, which drives ion transduction upon mechanical stress, enables the direct use of polymer ionogels as a piezo-electrolyte, eliminating the need for introducing inorganic piezoelectric materials.[33]

Herein, the mechanism of energy conversion and storage of SCPSs will be briefly discussed from the origin of piezoelectricity to the piezo-driven electrochemical process. The emphasis will be on the selection of polymer and polymer composite materials for the SCPS. We will present recent research advances classified based on functions and discuss their self-charging properties. Challenges and perspectives will be presented in the Conclusion section.

Fig. 1 Schematic diagram of the all-in-one piezo-driven self-charging power system. Reproduced from ref. 23 with permission from Elsevier, copyright 2018; reproduced from ref. 24 with permission from Elsevier, copyright 2019; reproduced from ref. 25 with permission from Wiley-VCH GmbH, copyright 2017; reproduced from ref. 26 with permission from American Chemical Society, copyright 2019.

2. Working principle of SCPSs

2.1 Introduction to piezoelectricity

The origin of piezoelectricity can be traced back to Maxwell's equations. As defined using Ampère-Maxwell's equation (eqn (1)), the displacement current J_D is produced by a time-varying electric field, rather than a current of moving charges. Piezoelectricity, also termed the piezoelectric effect, is actually part of the displacement current in Ampère-Maxwell's equations, which arises from the slight motion of charges confined within atoms (also known as dielectric polarization).[34]

$$\nabla \times H = J_f + J_D \quad (1)$$

$$J_D = \frac{\partial D}{\partial t} = \varepsilon_0 \frac{\partial E}{\partial t} + \frac{\partial P}{\partial t} \quad (2)$$

In eqn (2), the former part of J_D is the current due to the varying external electric field E, which gives rise to electromagnetic waves (radio, Wi-Fi, *etc.*) (eqn (2)). The latter part is induced by the varying surface charges P, which applies for piezoelectricity. Some materials can generate electric dipoles along with an electric field created by applied external mechanical force. Materials with this unique property are called piezoelectric materials, which are the key active materials of PENGs.[35] Piezo-materials create electrical outputs that are directly proportional to the applied stress upon mechanical

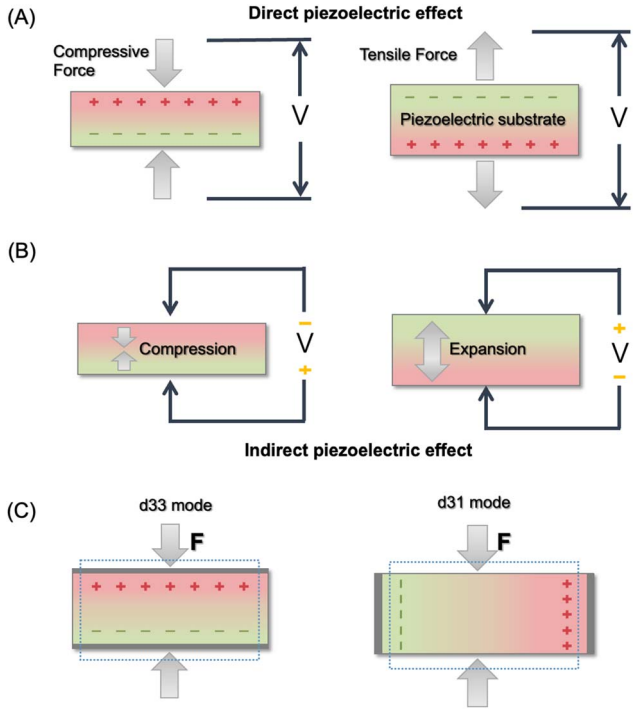

Fig. 2 Illustration of the direct piezoelectric effect (A), indirect piezoelectric effect (B), and two operation modes for piezoelectricity (C).

deformation, a phenomenon known as the direct (or inverse) piezoelectric effect (Fig. 2A). Its inverse process, in which the mechanical stress is generated in a piezo-material upon the applied electrical field, is termed the indirect (or converse) piezoelectric effect (Fig. 2B).[36] The equivalent circuit of the PENG can be represented by capacitors connected to a current source. The generated energy W can be calculated usingw

$$W = \frac{1}{2}QV = \frac{1}{2}(d\cdot\sigma\cdot A)(g\cdot\sigma\cdot e) = \frac{1}{2}d\cdot g\cdot\sigma^2\cdot V \qquad (3)$$

here d and g are the current and voltage constant coefficients, σ is the loading stress, V is the volume between the parallel plates, and Q is the accumulated charge. There are two operating modes for piezoelectricity, "33" and "31" (where the numbers 3 and 1 indicate the spatial dimensions), which are based on the direction of polarization and stress (Fig. 2C).[37] The 33 mode, evaluated using piezoelectric coefficient d_{33}, depicts induced polarization in the z axis direction by stress applied in the z axis. In the 31 mode assessed using piezoelectric coefficient d_{31}, the electric polarization is created along the z axis, perpendicular to the direction (x axis) of the applied stress. Generally, the value of d_{33} is higher than that of d_{31} for most of the piezoelectric materials; therefore d_{33} mode becomes dominant for most piezoelectric devices.[36,38,39]

2.2 Mechanism and configuration of the self-charging power system

The concept of the self-charging power system was proposed based on extensive studies of PENGs. An energy storage unit associated with an energy harvester accumulates ambient energy and outputs it on demand. When an energy harvesting unit is integrated into an energy storage system, the energy consumption of the device may be simply compensated *via* the conversion of ambient energy without the need for an electric recharging process. The first integration of an energy harvester and an energy storage device was implemented by Bae *et al.*, in which a PENG and supercapacitor were connected *via* an external circuit.[40] Since then, various prototypes of self-charging power systems have been developed, including separated module and all-in-one integrated design. For a self-charging power system with separate-module design, the energy generated by the piezoelectric nanogenerator (PENG) is collected and stored in an external energy storage module (Fig. 3A).[13,41,42] The direct piezoelectric output current signal of the PENG is normally irregular and even pulsed because of the randomness of the ambient kinetic energy and the apply/release cycle of the stress. Owing to the deformation–release cycle, the PENG generates an AC pulsed signal, which requires the DC conversion to power external loadings. Therefore, a management circuit, usually a full-bridge rectifier, is required between the harvester and energy storage module.[42]

The self-charging power system with separate-module has complicated configuration. The external connection between energy storage and rectification units results in unnecessary energy loss because of increased internal resistance. The rigidity of the management circuit is also unfavorable for the flexibility and durability of the device. Such low-level integration also leads to increased weight and reduced integration of the fabricated device. In response, a highly integrated all-in-one self-charging power system (abbreviated as SCPS) which can simultaneously convert ambient mechanical energy and store it in the form of electrochemical energy without any rectification circuit has become a reality (Fig. 3B).[17,43] In 2012, Xue *et al.* first developed an all-in-one self-charging power system (SCPS), which integrates an energy-harvesting piezoelectric nanogenerator (PENG) and an energy-storing lithium-ion battery (LIB) within a single coin-type cell.[17] Later on, the incorporation of a PENG and supercapacitor, most of which were flexible prototypes, was reported. For such an all-in-one SCPS, piezoelectric materials, mainly polymer-based materials, are used either as piezo-separators or solid piezo-electrolytes to substitute for their conventional counterpart. The working principle of the SCPS based on batteries and supercapacitors can be explained on the basis of the piezo-electrochemical process.[44,45]

At the initial stage without an external force (by pressing or bending), no electrochemical reaction occurs in the SCPS because of electrochemical equilibrium. When compressive force is applied, a piezoelectric potential is generated across the piezoelectric separator or solid-state electrolyte at the interfacial surface between the electrode and piezoelectric component, which breaks the electrostatic equilibrium. In battery-type SCPSs, the migration of Li^+ or Na^+ ions from the cathode to the anode is then induced by the piezo-potential (Fig. 4A). A similar process occurs in supercapacitor type SCPSs, in which the electrolytic ions (H^+, K^+, SO_4^{2-}, *etc.*) shuttle between two electrodes directed by a piezoelectric field. The induced electrochemical reactions in the bulk (battery), accumulation of

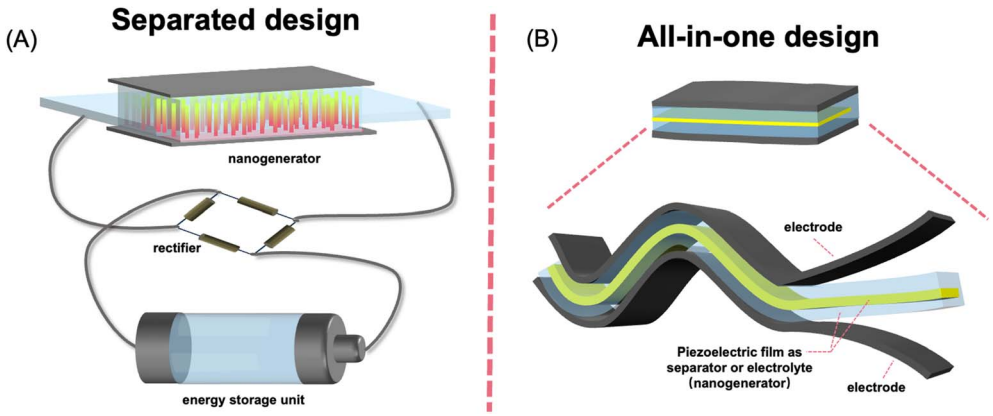

Fig. 3 Schematics of separate designed (A) and all-in-one (B) piezo-driven self-charging power systems.

ions (electrochemical double layer capacitors, EDLC) or fast surface redox reactions (pseudo-capacitor) enable the charging process.[17,46] Interestingly, upon removing the applied force, only a small amount of ions migrates reversely, and no net current flows in the opposite direction. Therefore, the connecting circuit and the rectifier between the harvester and energy storage unit are no longer required in such all-in-one SCPSs. The explanation of this rectification-free process in piezo-driven self-charging remains inconclusive. It has been proposed that upon the release of external compressive stress, a reversed piezoelectric field is created, albeit with a smaller magnitude compared to the compression state due to the lower strain rate in the relaxation process.[47] It is also reported that the piezo-electrolyte film continues to produce piezoelectric potential to enable self-charging for a period even after the external force is removed, attributed to residual strain during slow relaxation.[48] In this scenario, charge carrier ions migrate reversely towards their original position, leading to self-discharge. However, the reversed piezoelectric field cannot counteract the previous forward one in the self-charging process. Successful charging of the SCPS can be achieved as long as the frequency of the mechanical vibration exceeds a critical value.

Very recently, a piezoelectric ion (or piezo-ionic) effect induced self-charging process was proposed, which is slightly different from the abovementioned piezo-electrochemical mechanism.[33,49,50] The piezo-ionic effect depicts the separation of cations and anions in certain materials (*e.g.* ionogels) upon applied mechanical forces, resulting in the generation of a voltage or current.[51–53] Specifically, the pressure gradient in response to the applied force leads to a fluidic flow that drives ionic species. Subsequently, time-varying ion separation is induced due to different ionic mobilities, resulting in ionic voltage or current.[54] In flexible SCPSs, piezo-ionic polyelectrolytes are used as an ion source and a piezo-separator as well. Taking a Nafion based piezo-ionic self-charging supercapacitor as an example, the protons bound on the sulfate group in the equilibrium state move towards the elongated region on the supercapacitor electrode upon external stimulation (Fig. 4B).[55] The protons move *via* the tunneling effect between the sulfonic groups inside the ionomeric cavity of Nafion.[56] The adsorbed protons form an electric double layer at the electrode surface; subsequently, the resulting net potential triggers the self-charging process.

3. Key materials for polymer-based piezoelectric films

Since piezo-driven SCPSs are analogous to piezoelectric nanogenerators (PENGs), the most effective way to improve the self-charging capability is to enhance the output piezo-potential and

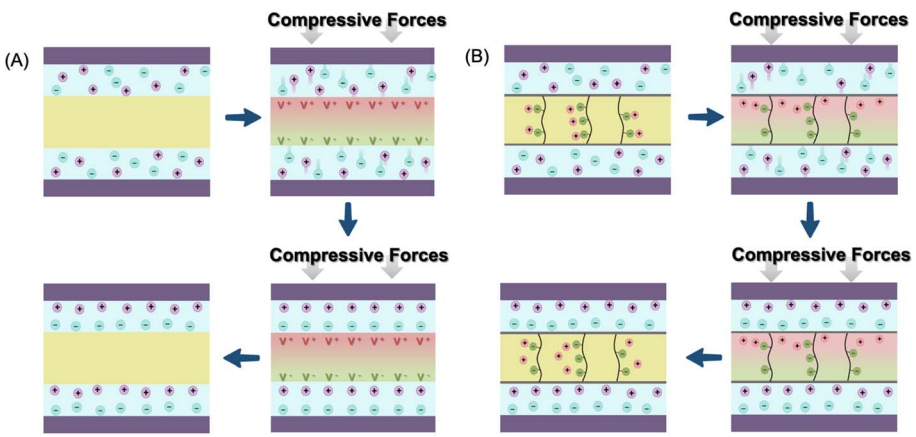

Fig. 4 Schematic illustration of the proposed mechanism for piezo-electrochemical (A) and piezo-ionic (B) processes.

enlarge the current density of the piezoelectric component as verified in PENGs. Considering the relatively low piezoelectric coefficient of polymeric piezo-materials and the use of other non-piezoelectric polymer matrices, it is imperative to enhance the piezoelectric response through hybridization or structure engineering. In this section, the polymer- or polymer composite-based piezoelectric films for PENGs are summarized to provide inspiration for exploring key materials in SCPSs. They mainly include PVDF and its copolymers, PVDF composites with 2D materials and piezoelectric inorganic materials, polyacrylonitrile (PAN) and non-piezoelectric polymer-based piezoelectric composites.

3.1 PVDF based piezoelectric films

PVDF and its co-polymers have the merits of good flexibility, mechanical robustness, chemical resistance and biocompatibility. They are promising materials for use as a piezoelectric component in SCPSs. PVDF based films have been extensively studied as battery or supercapacitor separators due to their tunable porosity, film-forming ability, chemical stability and permeability.[57,58] PVDF is also considered an ideal matrix for polymer solid-state electrolytes owing to its high relative permittivity, toughness, wide electrochemical window and long-term working temperature.[59] Moreover, PVDF and its copolymers such as P(VDF-TrFE) ($d_{31} = \sim 25$ pC N^{-1} and $d_{33} = \sim -30$ to -40 pC N^{-1}) have the best piezoelectric response among the reported piezoelectric polymers.[60,61] The crystalline phase of PVDF has a decisive influence on piezoelectricity. Among the three main phases (*i.e.* α, β and γ), the β and γ phases make a major contribution to piezoelectricity because of their polarity, while the β phase presents the largest electric dipole moment. Therefore, one of the key strategies to enhance the piezoelectricity is to increase the content of the β-phase in PVDF. This can be realized by stretching, thermal annealing and filler incorporation.[62–65]

Singh *et al.* utilized PVDF in the fabrication of a stretchable and lightweight piezoelectric sensor *via* an electrospinning process. The strong electric field and stretching force applied in the electrospinning technology induced β phase transformation and the $-CH_2/-CF_2$ dipole alignment of PVDF.[60,66] During the electrospinning process, the PVDF nanofibers aligned along the rotational direction, resulting in a significant increase in crystallinity (49%) and a substantial enhancement of the β phase (76.2%).[67] A nanoporous PVDF array was fabricated by the template-assisted preparation method which used Si pillars or vertically aligned, hydrothermally synthesized ZnO as the template (Fig. 5A). Harvesting from sonic waves, the robust porous PVDF PENGs generated a power density of 0.17 mW cm^{-3}, and the piezoelectric potential and piezoelectric current were enhanced 5.2 times and 6 times, respectively, compared to those from bulk PVDF films (Fig. 5B and C).[68] Maity *et al.* fabricated a self-powered piezoelectric sensor featuring highly aligned arrays of polyaniline-coated electrospun PVDF nanofibers (Fig. 5D).[69] The superior high content of β phase PVDF up to 99% endowed the device with a promising mechanosensitivity of 0.8 V kPa^{-1} and an excellent energy conversion efficiency of 53%. Additionally, the piezo-sensor also presented a sustainable energy harvesting capability. It exhibited a short-circuit current density of 4 μA cm^{-2} under a $\sim$10 kPa pressure by the human finger (Fig. 5G). The rectified maximum output power density was about $\sim$7 μW cm^{-2} under $\sim$10 kPa applied stress.

A PVDF-TrFE film has a better piezoelectric response and thus achieved higher electrical outputs than a PVDF film.[70] A robust PVDF-TrFE thin film fabricated *via* a facile and low-cost spin-coating technique on a polyimide substrate was used as a functional layer for flexible PENGs.[61] The obtained nanogenerator demonstrated an open-circuit voltage of up to 7 V and a short-circuit current of 58 nA, with a current density of 0.56 μA cm^{-2} at each stretching–releasing cycle. Both the measured open-circuit voltage and short-circuit current exhibited an increase in accordance with the strain rate. Highly oriented P(VDF-TrFE) fibers were initially prepared through electrospinning, followed by mechanical stretching.[71] The ordered, 80% aligned fibers induced by stretching enhanced piezoelectric properties, resulting in a greatly increased output voltage of 84.96 mV, which was more than 1.5 times higher than that of randomly distributed fibers. The mechanical durability of such highly oriented P(VDF-TrFE) fibers was also strengthened. Thanks to the abovementioned features, integrating P(VDF-TrFE) fibers into clothing can enable various motion-monitoring technologies.

3.2 PVDF composite piezoelectric films

The piezoelectric output produced by neat PVDF-based polymers, even after annealing or poling processes, is still relatively low with respect to many practical requirements. The incorporation of additives or fillers into PVDF is a straightforward and efficacious approach to improve its mechanical-to-electrical energy conversion efficiency.[35,72] Piezoelectric nanofillers directly enhance the piezoelectric output of composite films when incorporated with the PVDF matrix. Other nanofillers such as some 2D materials, although lacking the piezoelectric effect, can induce the β-phase transformation of PVDF for enhanced piezoelectric response.[73,74] In general, the roles of nanofillers include but are not limited to enhancing piezoelectricity, modulating dielectric properties, constructing conductive pathways, acting as stress concentrators, *etc.*[75] The commonly incorporated fillers include metal oxides,[76] lead-based piezoelectric materials,[77] lead-free piezoelectric ceramics [78] and 2D materials.[79]

3.2.1 PVDF/piezoelectric ceramic composites. Conventionally, the dominant ceramic piezoelectric material is commercially available lead zirconate titanate (PZT), which has a high d_{33} up to approximately 600 pC N^{-1}.[23] Hence, PZT-type materials, particularly in the form of zero-dimensional nanoparticles, have been extensively employed as fillers in PVDF-based composites for a myriad of piezoelectric devices.[77,80–82] The PVDF-PZT nanocomposite fibers were prepared *via* electrospinning.[77] The effect of the volume fraction of PZT on the β-phase content of PVDF was systematically evaluated. The dielectric constant, piezoelectric constant, piezoelectric

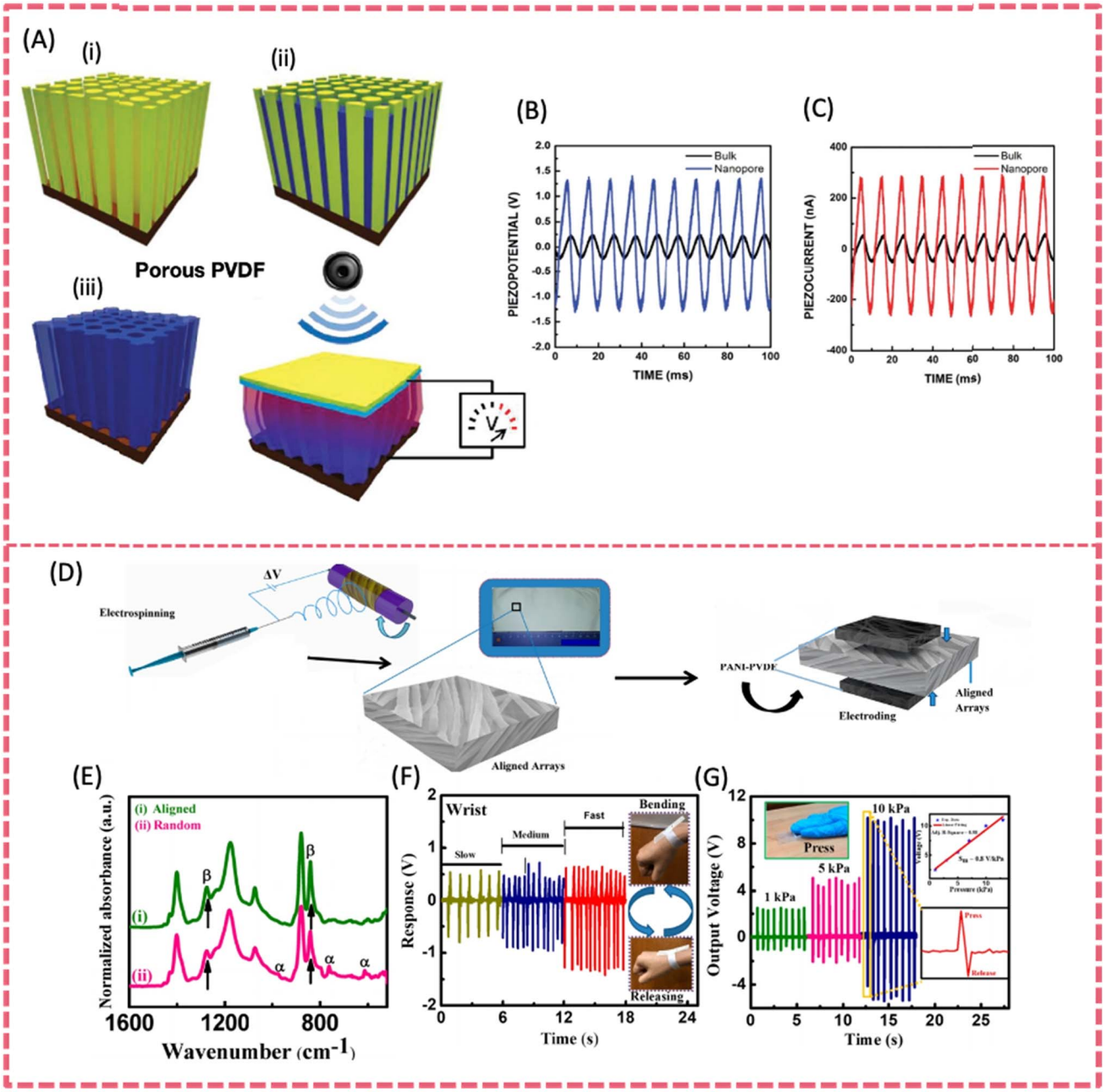

Fig. 5 (A) Fabrication process of a narrow nanoporous PVDF array by the template-assisted method. (B) Piezoelectric potential and (C) piezoelectric currents from the porous PVDF and bulk structure under the same force. Reproduced from ref. 68 with permission from American Chemical Society, copyright 2011. (D) Fabrication process of a piezo-organic e-skin sensor made of highly aligned PVDF NF arrays. (E) FT-IR spectra of aligned and random PVDF NF arrays. (F) Signal-responses of wrist bending. (G) Open-circuit output voltage responses under hand punching. Reproduced from ref. 69 with permission from American Chemical Society, copyright 2020.

sensitivity, and output voltage were enhanced along with the increased PZT ratio. The piezoelectric coefficient and output electrical voltage were increased from 10.51 pC N^{-1} and 22 mV (PVDF with 0.11 PZT) to 22.93 pC N^{-1} and 184 mV (PVDF with 0.37 PZT). To further enhance the piezoelectric properties, a rich lamellar baklava structure PZT/PVDF film was prepared *via* phase separation followed by a hot-press process (Fig. 6A), which benefits enhanced piezoelectricity, better access to external stress and faster signal response. [77] The composite film was able to output a V_{oc} and an I_{sc} of 2.51 V and 78.43 nA, respectively (Fig. 6C and D). The sensor based on such a composite film exhibited high sensitivity (6.38 mV N^{-1}) and rapid response (<21 ms), which can be used for self-powered wireless real-time monitoring systems.

However, the toxicity of lead in PZT limits the application of piezoelectric devices in bioelectronics. Therefore, lead-free piezoelectric materials including $BaTiO_3$ (BTO), $K_{0.5}Na_{0.5}NbO_3$ (KNN) and $Na_{0.5}Bi_{0.5}TiO_3$ (NBT) have been developed. They have

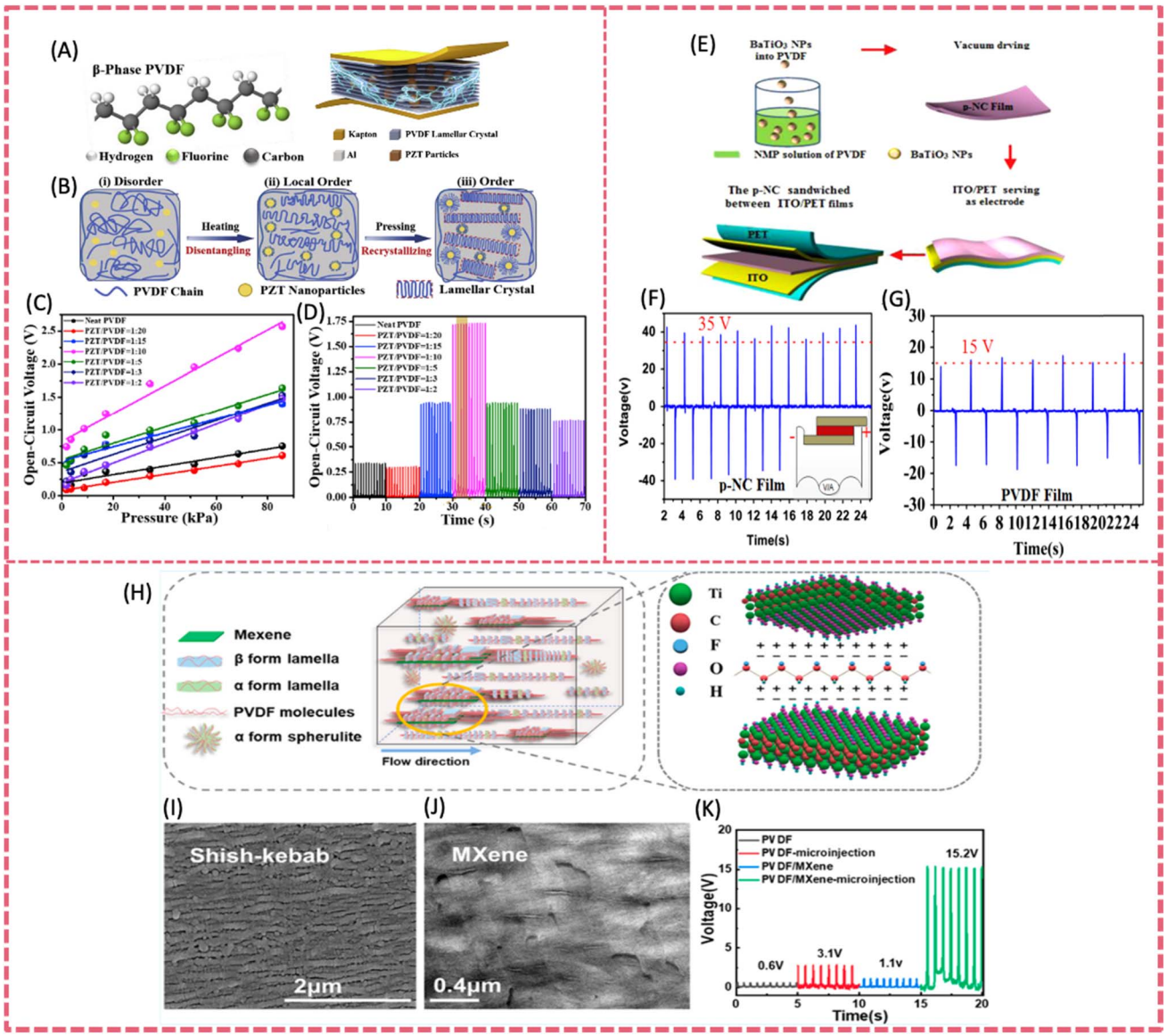

Fig. 6 (A) The general illustration and detailed structure of the PZT/PVDF composite sensor. (B) The conception of preparing a β-phase lamellar crystal. (C) Open-circuit voltage responses of the composite in a range of increasing pressures. (D) Open-circuit voltage varies with different contents of PZT particles under 34.23 kPa. Reproduced from ref. 80 with permission from Elsevier, copyright 2019. (E) The fabrication procedure of flexible piezoelectric nanocomposite nanogenerators. (F) The open-circuit voltage of the piezoelectric nanocomposite nanogenerators under 1 MPa stress. (G) The open-circuit voltage signals generated from the pure PVDF film NG under a stress of 1 MPa. Reproduced from ref. 83 with permission from Elsevier, copyright 2015. (H) Crystalline structure of the microinjected PVDF/MXene composite. (I and J) SEM image of the PVDF/MXene microinjected specimens. (K) The maximum open-circuit voltage generated by different samples. Reproduced from ref. 79 with permission from American Chemical Society, copyright 2021.

demonstrated comparable performance to lead-containing piezoelectric materials.[84–87] Lead-free piezoelectric ceramics are environmentally friendly and have greater potential in bio-related application when combined with PVDF. Among them, biocompatible BTO is an excellent lead-free piezo-material for its easy processability and outstanding piezoelectric properties. A BTO-PVDF film was prepared by incorporating BTO nanoparticles (BTO NPs) into a PVDF matrix *via* facile and scalable solvent evaporation in combination with a poling process (Fig. 6E).[83] The uniform distribution of BTO NPs and the oriented structure enabled the realization of an open-circuit voltage of 150 V and a short-circuit voltage of 1500 nA, which was one of the highest values among lead-free piezoelectric films (Fig. 6F and G). Additionally, the stress concentration of the polymer matrix originated from NP fillers also contributed to the enhanced power output. Adopting electrospinning technology for the preparation of PVDF composite films is a more promising method for the formation of the PVDF β-phase compared to electric poling.[88] The electrospun PVDF-$BaTiO_3$ (ES PVDF-BTO) composite nanofibers were developed to construct a high-output flexible PENG. The piezo-active crystalline phase of PVDF was further escalated due to the interfacial interaction

between the BTO fillers and polymer during electrospinning. Owing to the high β-phase content up to 91% and the addition of 10 wt% BTO, the resultant flexible PENG delivered an open-circuit voltage of ~50 V and a short-circuit current density of ~0.312 mA m^{-2}. Ponraj *et al.* employed KNN fillers with varying length scales in PVDF to investigate the influence of crystallite size (over a wide range) on the dielectric and piezoelectric properties of composite films produced by hot-pressing.[89] Due to the enhanced dipole–dipole and ion–dipole interactions between β-PVDF and KNN, a higher d_{33} value of 35 pC N^{-1} was presented containing 70 vol% micron-sized KNN particles. Teka *et al.* prepared PVDF/KNN composite filaments using the melt-spinning process and then fabricated flexible nanogenerators based on nanocomposite fiber mesh using electric poled PVDF/KNN.[78] The composite with 4% KNN showed the highest β content of 26%. The corresponding nanogenerator using PVDF/4%KNN delivered an output voltage and current of 3.7 V and 0.326 μA, respectively.

Among II–VI piezoelectric semiconductors, ZnO has the highest piezoelectric coefficient and offers the advantages of excellent electrical properties, low-cost, high abundance and chemical stability.[90–92] Moreover, nanostructured ZnO can be facilely grown on hard or flexible substrates to adopt to a broad variety of scenarios.[93,94] Vertically aligned ZnO nanorods were embedded into PVDF to obtain a PVDF-ZnO composite film *via* simple drop casting.[76] The vertically aligned ZnO induced the formation of β-phase PVDF, leading to an 1800 times enhanced power output compared to bare PVDF without electrical poling. Apart from ZnO nanowires or nanorods, the impregnation of ZnO nanoparticles (NPs) into the PVDF matrix also results in an increased content of the β-phase.[95] It was presumed that the negative surface charge in NPs had a catalytic effect promoting the nucleation of the polar β-phase in PVDF at an optimum volume ratio. The β crystal nucleation was enhanced to over 80%, and the corresponding piezoelectricity was increased to ~50 pC N^{-1} (d_{33}) at 50 Hz. The PENG based on PVDF-ZnO NPs presented a superior and enhanced output of V_{oc} ~24.5 V and I_{sc} ~1.7 μA and a remarkable power density of ~32.5 mW cm^{-3}.

3.2.2 PVDF/2D materials composites. The intrinsic piezoelectricity of some 2D materials such as h-BN, MoS_2 and GaS was theoretically predicted as early as the late 2000s.[96–98] The experimental verification of the piezoelectric effect in 2D materials was first reported by Wang's group in 2014.[99] Several theories have been proposed to explain the fundamental theory of piezoelectricity in 2D materials. The 2D forms of conventional piezoelectric materials present enhanced piezoelectricity compared to their bulk counterparts.[100] In another scenario, the bulk form of most common 2D piezoelectric materials such as (h-BN), transition metal dichalcogenides (TMDCs), group-III monochalcogenides and group IV monochalcogenides does not exhibit piezoelectricity. The strong piezoelectric coupling of the abovementioned 2D materials was predicted based on the calculation of piezoelectric coefficients using first-principles studies.[101] For instance, regarding hexagonal structured materials with a *D*6h symmetry and layered orthorhombic structured materials with a *D*4h symmetry, their two-dimensional monolayers exhibit inversion asymmetry because the structures are changed to the *D*3h group, leading to in-plane piezoelectricity.[102] More specifically, for few-layered h-BN and MoS_2, in-plane piezoelectricity was only found in an odd number of layers, because the materials with an even number of layers are centrosymmetric.[103]

A graphene/PVDF nanofiber was prepared by electrospinning a graphene oxide (GO) incorporating PVDF precursor. The piezoelectric output of the PENG base on graphene/PVDF nanofiber was significantly enhanced, owing to higher conductivity and β phase content induced by the incorporation of graphene. The β phase of the composite fibers containing 2 wt% GO (or rGO) was about 87%. Such a composite film was assembled into a flexible PENG, achieving a short-circuit current of 700 nA, an open circuit voltage of 16 V and a charge value of 5 nC, which were 20 times higher than that based on pure PVDF.[104] Nardekar *et al.* first prepared 1 T-MoS_2 quantum sheets with ultra-low dimensions (5–10 nm) in a 1–5 layer thickness by ball-milling.[105] These MoS_2 quantum sheets (QSs) were then incorporated into the PVDF matrix to fabricate a photovoltaically self-charging cell and piezoelectric nanogenerator. At a threshold MoS_2 QSs ratio of 7.5 wt%, the PENG showed an output voltage of ~34 V, much higher than that of pristine PVDF (5 V) and bulk MoS_2 (8 V). Under an applied force of 2 N, a rectified maximum output voltage of 32 V and a power density of 32 mW m^{-2} were recorded at a loading resistance of 0.830 GΩ. The PENG was able to charge a dielectric capacitor up to 0.7 V and lit up a LED bulb. The addition of some foreign polar 2D fillers can promote the polarization of PVDF due to the strong interaction between PVDF and the filler, and therefore the energy- and time-consuming post-poling process is no longer needed.[106,107] Han *et al.* reported a PVDF/MXene PENG *via* the microinjection molding process (Fig. 6H).[79] The intense shear force and stacked MXene sheets with numerous polar C–F groups not only promoted the formation of β-phase PVDF, but also induced regular arrangement of dipoles to produce a self-polarization effect. One of the microinjected composites iMP-1-400 containing 1 wt% MXene could reach a 93.4% relative content of β-phase PVDF. The piezoelectric charge constant and the voltage coefficient was 3.6 pC N^{-1} and 0.45 pC N^{-1}, respectively. The resultant flexible PENG provided an open-circuit voltage of 15.2 V and a short-circuit current of 497.3 nA (Fig. 6K).

3.3 Non-PVDF based piezoelectric films

3.3.1 Polyacrylonitrile piezoelectric films. Polyacrylonitrile (PAN) has been explored as the precursor for carbon fiber or battery separators for a long time.[108,109] Research on the piezoelectric properties of PAN was initiated only very recently due to the challenges associated with realizing its piezoelectricity.[110] The strong interaction between –CN groups induced the generation of 3^1-helical conformation, which has a lower sum of dipole moments and thus poor piezoelectricity.[111] Even with successful conformational modulation, maintaining the stability of the orientation of –CN groups to preserve a specific arrangement of dipoles under operational conditions remains a challenge. In response, several strategies have been

implemented to increase and maintain the zig-zag conformation in PAN, including the adjustment of fabrication and processing conditions and the incorporation of fillers. The mechanically oriented stress field generated during wet spinning can induce ordered alignment of PAN. Combined with a mechanical poling post-treatment, the orientation of PAN chains along the stretching direction is expected. The integration of high temperature and electric field can also enhance dipole alignment within polymers (*e.g.* PVDF), resulting in increased piezoelectricity.[31] However, such processing techniques are less effective when applied to PAN due to the unstable orientation caused by strong interaction among –CN groups.[111] Electrospinning is a widely applied processing technique to enhance the piezoelectric performance of piezoelectric polymers *via in situ* polarization and stretching induced by an electric field.[112] Lin's group reported unusually strong piezoelectricity in electrospun PAN by adjusting the electrospinning conditions (Fig. 7).[113] The main reason for this unexpectedly high piezoelectricity is the planar zigzag conformation, which can be tuned using rotary speed of the drum collector. As the linear velocity increased from 100 mm s^{-1} to 1800 mm s^{-1}, fiber alignment improved and the average diameter decreased. The maximum planar zigzag conformation contents were acquired at a speed of 1200 mm s^{-1}. The resultant PAN nanofiber mat generated a voltage of 2.0 V and a current of 1.0 μA, outperforming the PVDF mat fabricated under the same conditions. The tacticity of the polymer also plays a crucial role in affecting piezoelectricity in electrospun PAN. PAN with various levels of isotacticity can be obtained through radiation-induced polymerization of urea. Electrospun PAN with 25% and 52% isotacticity exhibited piezoelectricity with a d_{33} of 1–2 pC N^{-1}, whereas electrospun free-radical polymerized commercial PAN presented no piezoelectricity.[114] Furthermore, both isotacticity and planar zigzag conformation can be tuned by *in situ* polarization and stretching induced by the applied high electric field during electrospinning.[115] Hereafter, the integration of piezoceramics, semiconductors and inorganic salts with electrospun PAN was conducted to realize higher energy output,[116–118] as demonstrated for PVDF.

3.3.2 Non-piezoelectric polymer-based composite piezoelectric films. Except for PVDF and its-copolymer-based piezoelectric films, another facile approach is to integrate piezoelectric fillers with a non-piezoelectric polymer matrix (*e.g.* PVA) to prepare gel piezoelectric polymer electrolytes. From this point of view, the invention of high performance piezoelectrolyte relies on the hybridization of piezoelectric fillers and their interaction with the filler-polymer matrix. PVA-piezoelectric filler composite based PENGs were rarely reported. However, the examples of piezoelectric fillers composited with other non-piezoelectric polymers can also serve as good references. Inorganic piezo-materials applied in polymer-based PENGs are expected to have great potential in PVA composite piezo-films as well.[93,94]

Vertical ZnO NW arrays can be grown on arbitrary shaped substrates of any material *via* solution-based technology.[119,120] Since the as-grown vertical ZnO NW arrays naturally have

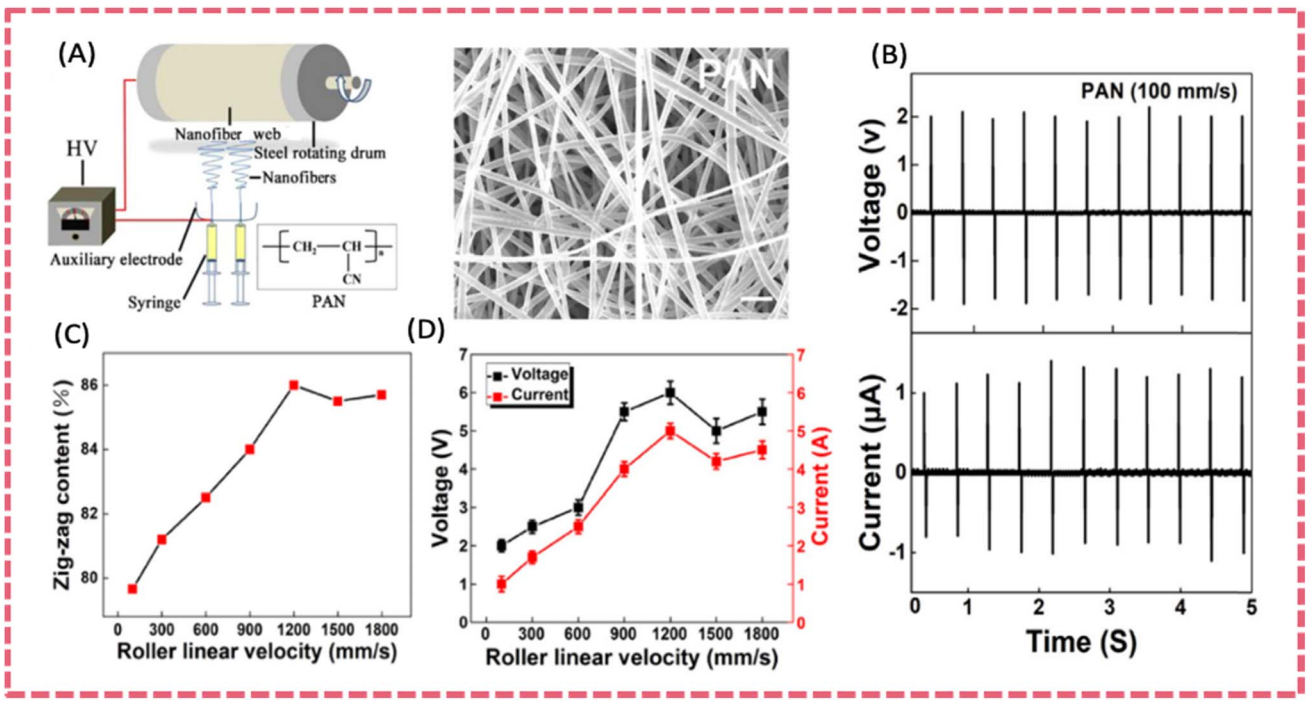

Fig. 7 (A) Electrospinning apparatus for producing PAN nanofiber membranes and SEM image of the as-spun PAN nanofibers. (B) Piezoelectric outputs of the nanofiber device under repeated compression impact (line speed 100 mm s^{-1}, frequency 2 Hz). The effect of collector drum rotation speed on (C) planar zigzag conformation contents (Φ) and (D) electric outputs of the energy devices. Reproduced from ref. 113 with permission from Elsevier, copyright 2019.

consistent polar directions along the *c*-axis upon applied strain, they can serve as piezoelectric fillers for polymer composite films.[41] PVA-ZnO nanocomposites with different ZnO nanorod (ZnR) alignments including unoriented, oriented, and hierarchical were prepared as hybrid triboelectric/piezoelectric nanogenerators (Fig. 8A).[121] When the ZnR orientally aligned along the *c*-axis, the composite exhibited the highest power output of 15.9 W m^{-2}, which was ~17-fold enhancement compared to pristine PVA (Fig. 8B and C). Such large piezoelectric polarization was due to the strengthened deformation under vertical compression enabled by highly oriented ZnRs. The performance of pristine ZnO can be improved by doping with III–IV group elements.[122] Sn-doped ZnO was prepared and then composited with PVA to obtain a thin composite film. With 2.5% Sn doping, the performance of the PVA/ZnO based PENG was enhanced by 2-fold at the maximum applied force. More specifically, the open circuit potential and short circuit current was increased to 4.15 V and 36 nA, respectively.

A self-powered PENG based on a PZT/cellulose (MFC)/PVA composite was fabricated by the melt copolymerization method (Fig. 8D).[123] PZT greatly enhanced the piezoelectricity and the introduction of MFC increased the elastic modulus and tensile strength of the film. The maximum output of the composite film was 3.3 μW (V_{oc} = 16.5 V, I_{sc} = 0.86 μA) (Fig. 8F). In addition, the composite film exhibited extremely high mechanical strength with a tensile strength of 41.9 MPa. Although there were very few studies on PVA-BTO and PVA-KNN films, composite films composed of lead free piezo-ceramics incorporated in other non-piezoelectric polymer matrices can be regarded as good references. Chen *et al.* developed a transparent and stretchable highly integrated PENG using spray-coated AgNWs as stretchable electrodes, BTO embedded PDMS as the piezoelectric sensing layer and a thin PDMS film as the protective and triboelectric layer.[124] The BTO-PDMS piezoelectric layer generated a typical output voltage of 2.8 V and a current density of 130 nA cm^{-2} under a compressive force of 50 N. Potassium sodium niobate (KNN) with recognized biocompatibility is another promising lead-free piezoelectric ceramic.[125,126] Using a sol–gel processing method, KNN piezoelectric films were coated onto flexible metal foil.[127] The flexible KNN@Pt film showed an improved piezoelectric coefficient d_{33} of 75.1 pm V^{-1}, which surpassed that of the rigid KNN film (52.8 pm V^{-1}). To improve the alignment of dipoles, Ag particles were attached on piezo-particles KNN and then mixed with carbon nanotube/PDMS to fabricate a PENG. The Ag/KNN PENG poled at 5 kV mm^{-1} and generated a maximum open-circuit voltage of 282 V and a short-circuit current of 32.2 μA under 10 kPa external mechanical stress.

4. Current advances in polymer piezoelectric films for SCPSs

A highly integrated SCPS is a device that combines the energy harvesting and energy storage components into a single unit.

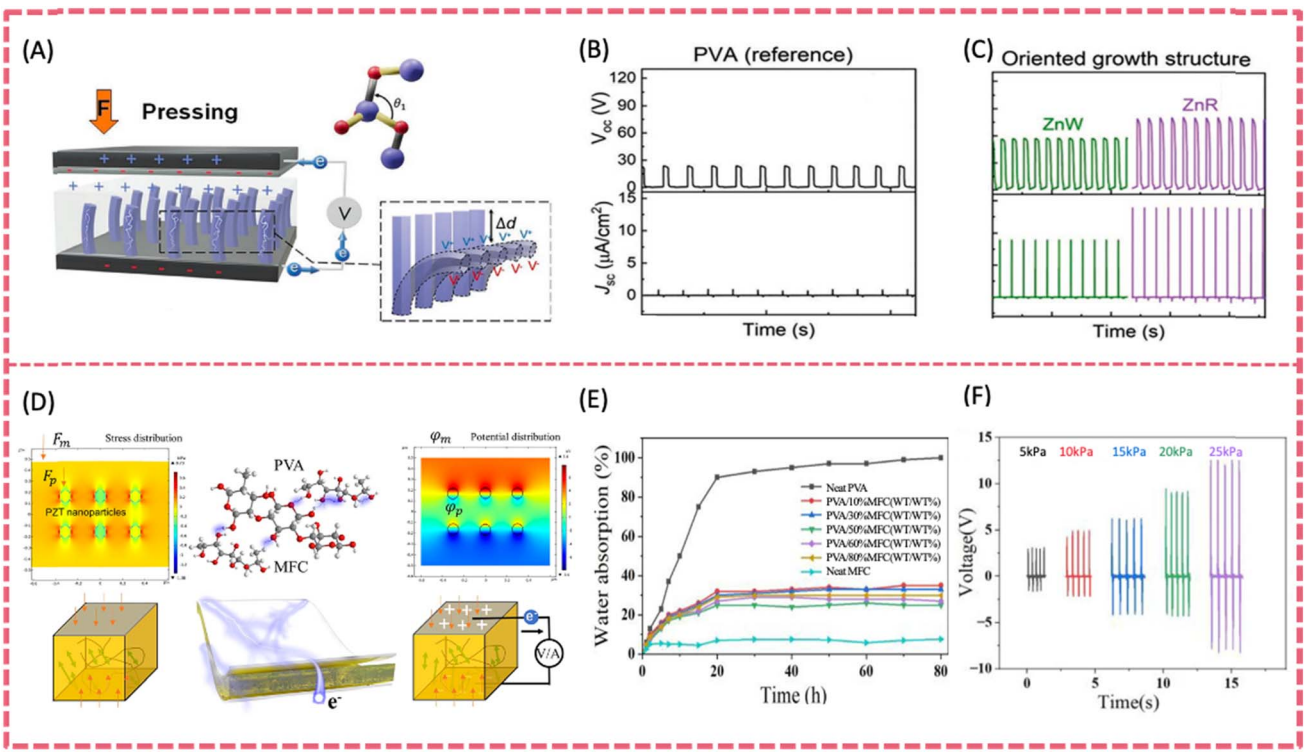

Fig. 8 (A) The working mechanism of H-P/TENG under externally applied force. The open-circuit voltage and short-circuit current density for (B) PVA as a reference and (C) oriented (ZnWs and ZnRs) at a constant applied force of 50 N. Reproduced from ref. 121 with permission from Wiley-VCH GmbH, copyright 2022. (D) The molecular structures of PVA and MFC and a PZT/MFC@PVA composite film and working principle of the PENG. (E) Water absorption of MFC@PVA composite films. (F) The output voltage curve under different stresses. Reproduced from ref. 123 with permission from Elsevier, copyright 2023.

The key material for such configuration is multifunctional polymer-based films, which serve as both a piezoelectric nanogenerator and a separator/electrolyte for energy storage devices. Some polymer films with intrinsic piezoelectric properties can be used as a battery/supercapacitor separator after appropriate structure design. It is facile to fabricate polymer piezoelectric electrolyte by incorporating piezoelectric nanoparticles/nanowires/nanofibers into conventional polymer solid-state/gel electrolyte or using polymer electrolyte with inherent piezoelectric properties. To date, various polymer-based multifunctional films have been demonstrated for SCPSs, which will be discussed in detail below. Also, the performance metrics of different SCSPCs reported are summarized in Table 1.

4.1 Polymer-based piezoelectric separators for SCPSs

A separator is an indispensable component for batteries and supercapacitors that physically separates the two electrodes, preventing the occurrence of a short circuit. Highly flexible polymer films with well-defined porosity are the most promising materials for separators. Currently, polyolefins (polypropene and polyethene) are the most used polymers for commercially available battery separators.[152] To further improve the electrochemical properties of batteries and overcome shortcomings such as limited wettability, low porosity and thermal shrinkage, polymers beyond polyolefins including poly(acrylonitrile) (PAN), poly(methylmethacrylate) (PMMA), poly(ethylene oxide) (PEO), and poly(vinylidene fluoride) (PVDF) and its copolymers have been explored.[153] Owing to the features of easy processability, chemical/electrochemical stability, controllable crystallinity and high dielectric properties, PVDF and its copolymer films have been extensively studied as separators.[154] Considering the outstanding piezoelectric properties, PVDF-based polymers emerge as a promising option for piezoelectric separators.

Generally, porosity is one of the most important parameters of polymer separators. Abundant porosity up to 40% is required to ensure the permeability of electrolyte.[155] Also, the pore size should be appropriate to prevent the penetration of electrode material particles and even lithium dendrites. Ideally, submicrometer-sized, evenly distributed and tortuous pores are favored for uniform current distribution and inhibition of Li dendrite growth. High wettability, sufficient electrolyte absorption, and excellent electrolyte retention of the separator are prerequisites for electrolyte infiltration and ion transport. The separator should also possess good mechanical strength including tensile strength and puncture strength, to withstand the strain during manufacturing and usage.[155] Excellent chemical and thermal stabilities are required for polymer separators as well. Chemical stability includes not only high resistance to oxidants, reductants and organic solvents, but also the ability to maintain mechanical strength during electrochemical processes. The separator must maintain its dimensions and physical properties over a wide temperature range without wrinkles and shrinkage. Besides, there are other requirements such as electrical insulation, minimal electrolyte (ionic) resistance, air permeability and safety.[155]

While the study of piezoelectric separators is still in the proof-of-concept stage, it is premature to discuss the above-mentioned significant separator parameters. As the research progresses, increasing emphasis will be placed on the electrochemical performance rather than solely on the piezoelectric properties of the separator. Exploring the impact of key separator parameters on the self-charging capability of the piezoelectric separator holds significant research value.

4.1.1 Polymer-based piezoelectric separators for self-charging batteries. The first proof-of-concept SCPS prototype was developed by Xue *et al.* in 2012,[17] in which a pre-polarized PVDF film was used to replace the conventional polyolefin separator in a coin cell type lithium-ion battery (LIB) (Fig. 9A). The self-charging process was driven by the piezoelectric potential generated by the PVDF film under pressing. Under a periodic compressive stress of 45 N at a 2.3 Hz frequency, the voltage of the cell was increased from 327 to 395 mV within 240 s, storing a capacity of 0.036 μAh (Fig. 9B). More interestingly, the integrated design demonstrated a higher mechanical-electrochemical energy conversion efficiency compared with the separated design consisting of a piezo-generator and an energy storage unit connected through a bridge rectifier. The device based on the latter design showed a voltage increase of only ~10 mV after being charged for 4 min *via* cycled deformation of the PVDF PENG. However, this self-charging (SC) Li-ion battery used rigid, coin-cell type design, which failed to maximise the piezoelectric output and was also unsuitable for wearable devices. Later in 2014, the first flexible self-charging battery using Kapton film as a supporting shell was reported.[129] The SC-LIB consisted of a $LiCoO_2$ cathode, graphene anode and pre-polarized PVDF piezo-separator (Fig. 9C). Such flexible design can fully utilize the external mechanical stress in comparison to its counterparts with a rigid shell, leading to higher piezoelectric potential. It was charged from 500 mV to 832 mV within 500 s under a periodic compressive stress of 34 N at 1 Hz, which was equal to a 0.266 μAh capacity (Fig. 9D). Also benefiting from the flexible structure, such a device was able to harvest and convert tiny environmental mechanical energy such as finger pressing or compression from bicycle tire rolling. Both materials optimization and device configuration design can boost the self-charging ability of the SC battery using a bare polymer piezo-separator. A porous, electrospun P(VDF-TrFE) film was used as both a flexible support matrix for the electrode and piezo-separator (Fig. 9E).[128] A hierarchical nano-microporous structure was created by introducing PEG into the electrospinning solution. The unique porous structure of the piezo-separator, along with a self-supporting electrode on a P(VDF-TrFE) substrate, endowed the SCPS with excellent flexibility and high piezo-driven self-charging performance. This SCPC without the use of liquid electrolyte can be considered a flexible PENG, which exhibited a maximum output voltage of 180 V at 30 Hz. At an external force of only 6 N at 1 Hz, the SCPC was charged from 70 to 240 mV within 330 s, demonstrating an excellent mechanical-electrochemical transduction ability under tiny mechanical deformation (Fig. 9G). Accordingly, this flexible SCPC exhibits great potential for collecting the tiny

Table 1 Performance metrics of reported piezo-driven self-charging energy storage systems

Materials	Methods	Device	Electrode materials	Specific capacitance	Self-charging force	Self-charging performance
Polarized PVDF film[17]	Purchase	Li-ion battery	Anode: TiO_2 nanotube arrays Cathode: $LiCoO_2$	0.36 mA h cm^{-2}, C/10 rate	2.3 Hz, 45 N, 240 s	327 to 395 mV, stored 0.036 μAh at 1 μA
P(VDF-TrFE)-PEG-TPU nanofiber[128]	Electrospinning	Li-ion battery	Anode: Graphite Cathode: $LiFeO_4$	139.9 mA h g^{-1}, 1C	1 Hz, 6 N, 330 s	70 to 240 mV, stored 0.092 μAh at 10 μA
Polarized PVDF film[129]	Purchase	Li-ion battery	Anode: Graphene Cathode: $LiCoO_2$	—	1 Hz, 34 N, 500 s	500 to 832 mV, stored capacity 0.266 μAh under 1 μA
Polarized PVDF-PZT[130]	Spin-casting	Li-ion battery	Anode: MWCNTs Cathode: $LiCoO_2$	—	1.5 Hz, 10 N, 240 s	210 to 297.6 mV, stored capacity 0.010 μAh at 1 μA
KNN@SEBS piezo-film[24]	Casting	Na-ion battery	Anode: Ni_2P@PNC Cathode: NVP@C	97 mA h g^{-1}, 11.7 mA g^{-1}	Palm patting (10 N, 2 Hz), 300 s	0.14 to 0.36 V and maintains the increasing trend until 0.65 V
PVDF-rGO-ZnO composite films[131]	Spin-coating	Supercapacitor	MnO_2-rGO	7.6 F g^{-1} at 0.01 mA cm^{-2}	Hand-tapping, 100 s	1.5×10^{-3} mC charge
Porous P(VDF-TrFE) foam[132]	Vapour-induced phase separation	Supercapacitor	CNTs	1.2 mF cm^{-2} at 0.05 mA cm^{-2}	5 Hz, 70 N, 40 s	70 mV increase, stored 95 mF cm^{-2} at 0.1 mA cm^{-2}
P(VDF-TrFE)-BTO [133]	Spin-coating	Supercapacitor	Positive: NiCoP/NiCoN heterostructure Negative: AC	3544 mF cm^{-1} at 1 mA cm^{-2}	35 N, 146 s	50 mV to 183 mV, storage capacity 0.094 μAh at 3 μA
Polarized mesoporous PVDF film[134]	Acid etching	Li-ion battery	Anode: Graphite Cathode: $LiCoO_2$	328.95 mA h g^{-1} at 0.3C after 30 cycles	30 N, 1 Hz, 240 s	25 to 473 mV, storage capacity 0.118 μAh at 5 μA
Siloxene-PVDF piezofiber[135]	Electrospinning	Supercapacitor	Siloxene	28.98 mF cm^{-2}, 5 mA	20 N, 250 s	107 to 314 mV
PVDF film[47]	Purchase	Supercapacitor	Functionalized carbon cloth	357.6 F m^{-2}, 8 A cm^{-2}	4.5 Hz, 40 s	100 mV increase, stored capacity 0.25 mA h at 100 μA
Fish swim bladder[136]	—	Supercapacitor	Positive: NiCoOH-CuO@Cu foil Negative: RGO@Cu foil	165.1 F g^{-1}, 1 A g^{-1}	16.4 N, 1.65 Hz, 80 s	130.1 to 281.3 mV, stored capacity 0.424 μAh at 10.5 μA
Fish scale[137]	—	Supercapacitor	Positive: MnO_2 Negative: Fe–Mn sulfide@rGO	93 F g^{-1}, 2 A g^{-1}	Finger imparting, 20 s	115 to 350 mV
PAN film[138]	Electrospinning	Supercapacitor	Activated carbon fabric	20 mA cm^{-2}, 2 mA cm^{-2}	30 N, 1.5 Hz	117.8 mV increase
BTO-P(VDF-HFP)[139]	Casting	Sodium-ion full battery	Anode: Carbon Cathode: $Na_3V_2(PO_4)_3$@C	70 mA h g^{-1} after 40 cycles at 10 mA g^{-1}	Repeated bending, 300 s	0.08 to 0.32 V and continue increasing to 0.40 V, stored capacity 0.304 mA h at 10 mA
KNN/PVA/H_3PO_4 piezo-electrolyte film [140]	Casting	Supercapacitor	Stretchable graphene/SEBS	167 μF cm^{-2}, 2 μA cm^{-2}	Palm patting (2 Hz), 300 s	Charged to ~1.0 V
PVA-KCl-BTO piezo-electrolyte[141]	Casting	Supercapacitor	Co-Fe_2O_3@ACC	2.86 mF cm^{-2}, 0.09 mA cm^{-2}	180° bending, 1 Hz, 7 min	6 to 120 mV
PVA/KOH/BTO piezoelectrolyte[142]	Casting	Supercapacitor	$NiCo_2O_4$@ACC	6.89 mF cm^{-2}, 0.120 mA cm^{-2}	180° bending, 1.5 Hz, 7 min	0.25 V increase
Nafion polyelectrolyte film[55]	—	Supercapacitor	Graphene sheets	245.02 mF cm^{-2}, 5 mA	Acceleration of 10 m s^{-2}, 300 s	42 to 383 mV
PTA-PVDF piezo-polymer-electrolyte film[143]	Casting	Supercapacitor	Graphene	184.94 mF cm^{-2}, 1.0 mA	2 N, 300 s	52 to 162 mV
PVDF-ZnO film[46]	Solution casting	Supercapacitor	MnO_2 nanowires	455 mF g^{-1}, 0.04 mA cm^{-2}	Palm impact, 300 s	35 to 145 mV (110 mV charged)

Table 1 (*Contd.*)

Materials	Methods	Device	Electrode materials	Specific capacitance	Self-charging force	Self-charging performance
PVDF/$NaNbO_3$ nanofibers[144]	Electrospinning	Supercapacitor	2D $MoSe_2$	18.93 mF cm^{-2}, 0.5 mA	30 N, 100 s	Up to 708 mV increase
P(VDF-TrFE) film[145]	Electrospinning	Supercapacitor	PDMS-rGO/C	44.6 μF cm^{-2}, 25 μA cm^{-2}	90° finger bended	0.45 V increase
Polarized PVDF film[146]	Casting	Supercapacitor	WS_2@PPy heterostructure	245 F g^{-1}, 1 A g^{-1}	Finger pressing, 60 s	A maximum output potential of 880 mV
Porous PVDF[147]	Acid etching	Li-ion battery	Anode: Graphite Cathode: $LiCoO_2$	—	282 mJ, 1 Hz, 200 s	1.2 to 1.4 V, stored capacity 0.4 μAh at 0.01 mA (1C)
MXene PVDF[148]	Casting	Supercapacitor	MXene	61.6 mF cm^{-2}, 0.2 mA	—	—
PVDF/sodium niobate[149]	Electrospinning	Supercapacitor	PVDF/reduced graphene oxide composite	683 nF cm^{-2}, 10 nA	40 N, 190 s	0.8 V increase
PVDF-HFP/PZT/TPU[150]	Electrospinning	Sodium-ion battery	Symmentric cathode: PVDF-HFP/NVP/TPU	44.1 μAh cm^{-2}, 10 μA cm^{-2}	Palm patting, 600 s	279.3 to 331.3 mV, stored capacity 0.083 μAh at 5 μA
PVA-KOH-CZTO[151]	Coating	Supercapacitor	Fe_2O_3-g-C_3N_4	141.3 F g^{-1}	9.47 N, 3.7 Hz (finger imparting), 180 s	669.2 mV increase

movement energy of the human body to power wearable electronic devices.

Exploring a new polymer separator with better piezoelectric properties is critical for boosting the self-charging capability. Polymer composite films, such as piezo-ceramic/polymer and 2D materials/piezoelectric polymer composite films, show potential for enhancing the piezoelectricity.[156] By hybridizing PZT with PVDF, the piezoelectric potential of the composite films can be intensified, and the physical properties may be changed. Yang *et al.* report a simple, effective and low-cost way to fabricate a PVDF-PZT nanocomposite film *via* spin-casting, which stored twice the capacity of a pure PVDF film (~0.010 *vs.* 0.004 μAh) as a piezo-separator in a $LiCoO_2$/MWNT coin-cell type LIB.[130] A similar composite piezo-separator was applied to fabricate a battery-type flexible SCPS. A flexible and SC sodium-ion full battery was developed by coupling the elastic composite piezo-separator with an $Na_3V_2(PO_4)_3$/C cathode and a Ni_2P/C anode (Fig. 9H).[24] The piezo-film was cast by incorporating KNN piezoelectric particles into a highly elastic SEBS film and then forming a bilayer separator with a glass fiber membrane. The flexible SC SIB exhibited an excellent self-charging behavior under bending (~60°) or palm patting (~10 N, 2 Hz) (Fig. 9I and J). It was easily charged from 0.19 to 0.28 V by bending in 150 s, and the self-charging continued to 0.65 V even after the bending stopped. Similarly, the voltage of the flexible SC SIB experienced a rapid increase from 0.14 to 0.36 V under palm patting for 300 s and maintained the increasing trend until ~0.65 V after external stress was removed. The hysteretic piezoelectric response can be attributed to the exceptional mechanical energy absorption and storage capabilities of the elastomer. Similarly, an all-in-one stretchable, self-chargeable sodium-ion thin-film battery was fabricated based on an electrospun PVDF-HFP/PZT/thermoplastic polyurethane (TPU) film and two symmetric electrospun $Na_3V_2(PO_4)_3$/C/TPU cathodes.[150] The stretchable sodium ion battery can achieve 279.3 to 331.3 mV under palm patting with 0.083 μAh stored capacity. The excellent stability of the self-charging behavior under repeated deformation could enable accumulative energy collection during practical use.

4.1.2 Polymer-based piezoelectric separators for self-charging supercapacitors. The relatively low output of self-charging makes it less likely to fully compensate for the energy required to fully recharge the battery. Therefore, the design and fabrication of self-charging supercapacitors (SCSCs) with relatively lower energy density are more promising. A flexible SCSC has a versatile design that meets the requirement of ambient working conditions and allows for a broadened selection criterion for materials. The piezo-electrochemical process is also the driving force for the self-charging of electrochemical double layer (EDLC) or pseudocapacitive supercapacitors.[135] A rectification-free, self-charging supercapacitor was first demonstrated in 2015 and consisted of a polarized PVDF separator, a functional carbon cloth electrode and H_2SO_4/poly(vinyl alcohol) (PVA) gel electrolyte (Fig. 10A).[47] When a compressive force was applied, the polarization of PVDF was changed and then a piezoelectric field was generated. Although a small reversed piezo-potential was created upon removal of

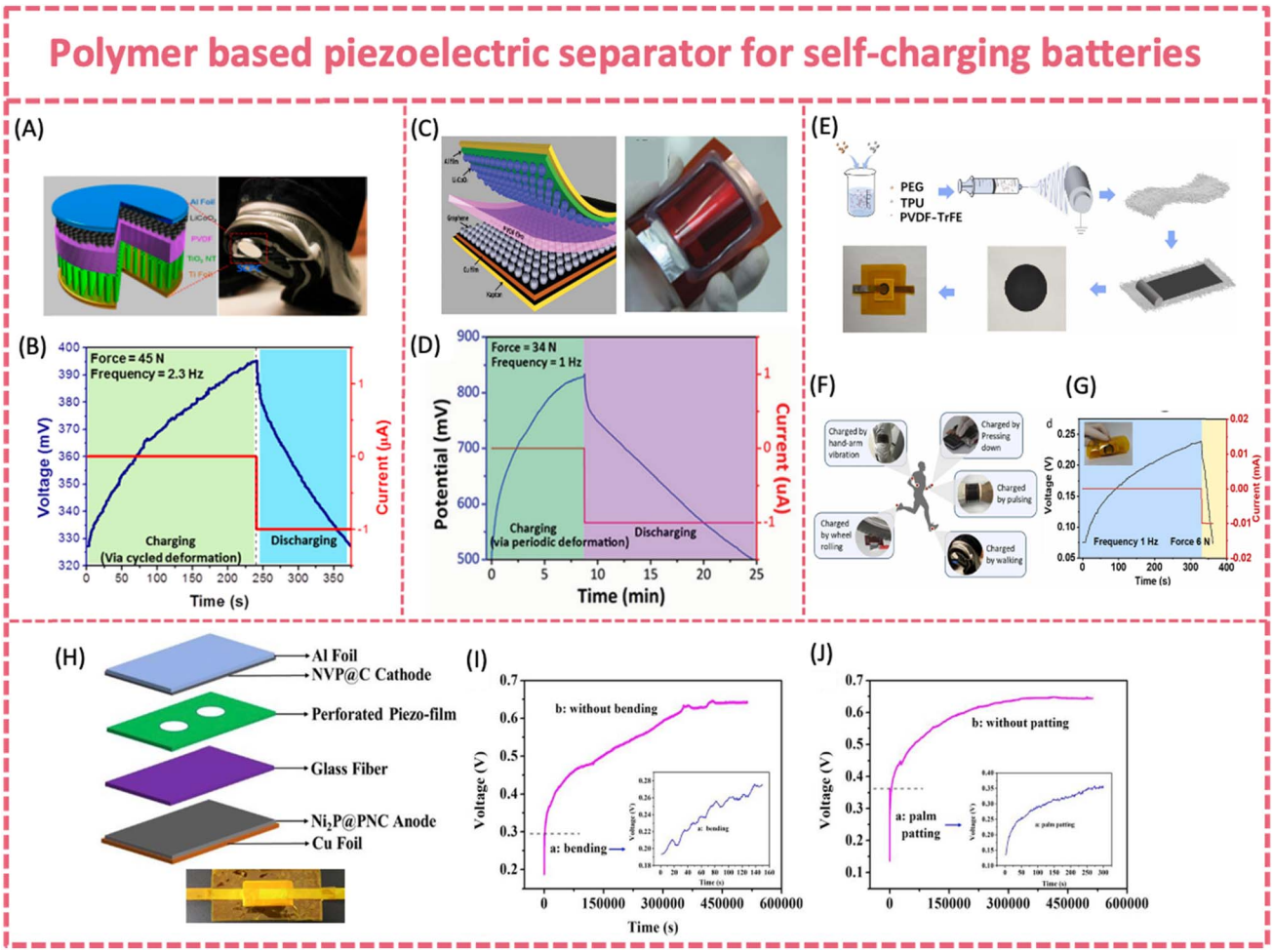

Fig. 9 (A) Structure and applications of a SCPC made of $LiCoO_2$ (cathode) and TiO_2 (anode) separated using a polarized PVDF membrane and (B) self-charging process under compressive force. Reproduced from ref. 17 with permission from American Chemical Society, copyright 2012. (C) Structure and optical image of the flexible SCPC made of $LiCoO_2$ (cathode) and graphene nanosheet composites (anode) separated using a polarized PVDF film and (D) self-charging process of the flexible SCPC under compressive force. Reproduced from ref. 129 with permission from Wiley-VCH GmbH, copyright 2014. (E) Fabrication procedure of the fully flexible SCPC; (F) possible applications of the SCPC to utilize biomechanical energy and (G) self-charging response of the fully flexible SCPC. Reproduced from ref. 128 with permission from Elsevier, copyright 2022. (H) Device architecture of the flexible SC SIB; (I) self-charging process by bending and (J) palm patting. Reproduced from ref. 24 with permission from Elsevier, copyright 2019.

compression, it could not counteract the overall self-charging process. The voltage of the device was increased to 100 mV within 40 s with an average frequency of 4.5 Hz, storing a capacity of 0.25 μAh (Fig. 10B). Parida *et al.* reported a poled porous P(VDF-TrFE) foam prepared by the vapor-induced phase separation method as a piezo-separator in a SC supercapacitor, which generated a voltage 3.5 times higher than that of a compact P(VDF-TrFE) film (Fig. 10C).[132] Upon an external compressive force of 70 N at a 5 Hz frequency, the SC device was charged from ~0 mV to ~60 mV within 10 s and finally reached ~70 mV with a stored capacitance of 95 mF cm^{-2} (Fig. 10D).

Similar to those in flexible PENGs and SC batteries, nanofillers such as ZnO, 2D materials and piezoelectric ceramics (PZT, BTO, and KNN) are introduced to enhance the piezoelectric output of PVDF based polymer piezo-separators. By adding ZnO nanoflakes and rGO into PVDF, a significant enhancement in the piezoelectric response was observed. It exhibited a maximum output voltage of 44 V, a current density of 1 μA cm^{-2} and a power density of 193.6 μW cm^{-2} (Fig. 10E and F).[131] The self-charging behavior of the flexible supercapacitor with the PVDF-ZnO-rGO piezo-separator showed a stored charge of 1.5×10^{-3} mC in only 84 s (~190 mV increases in potential) under a 5 N tapping force, without resorting to a rectifier. A porous P(VDF-TrFE)/BTO piezoelectric film was successfully fabricated through spin coating-polarization techniques. It was then assembled into a flexible solid-state self-charging supercapacitor power cell coupled with NiCoP/NiCoN and activated carbon electrodes (Fig. 10G and H).[133]

Under a 35 N compressive force at a 1 Hz frequency, the composite piezo-film with 50 wt% of BTO presented a V_{oc} and an I_{sc} of 14.2 V and 0.62 μA, respectively. The practical self-charging properties were characterized by a 133 mV voltage increase within 146 s under a 35 N force. 2D siloxene was

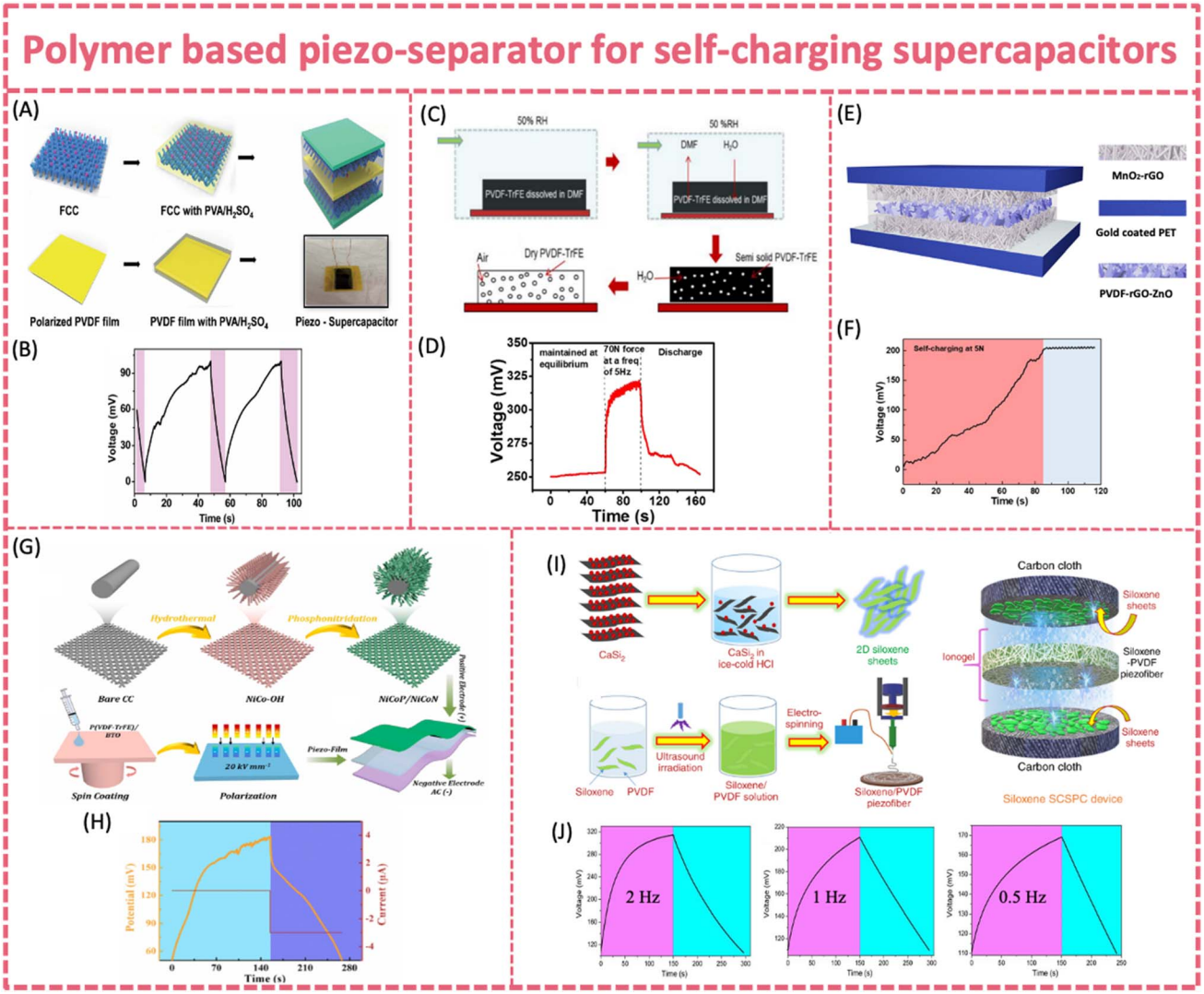

Fig. 10 (A) Fabrication process of a hybrid piezo-supercapacitor made of functionalized carbon cloth electrodes separated using PVDF and (B) self-charging process of the piezo-supercapacitor under a compressive force with an average frequency of 4.5 Hz. Reproduced from ref. 47 with permission from the Royal Society of Chemistry, copyright 2015. (C) Fabrication of the porous PVDF-TrFE film and (D) self-charging behavior of the SP-EDLC device. Reproduced from ref. 132 with permission from Elsevier, copyright 2017. (E) Fabrication of the SCPU device made of MnO_2-rGO heterostructure electrodes separated using PVDF-ZnO-rGO film and (F) self-charging test under a hand-tapping force. Reproduced from ref. 131 with permission from American Chemical Society, copyright 2020. (G) Fabrication process for the synthesis of a NiCoP/NiCoN heterostructure, P(VDF-TrFE)/BTO piezo-film and SCSPC device. (H) Self-charging properties of the SCSPC at a compressive force of 35 N. Reproduced from ref. 133 with permission from Elsevier, copyright 2022. (I) Overall process involved in the fabrication of a siloxene SCSPC. (J) Self-charging properties of the siloxane SCSPC at 2 Hz, 1 Hz, and 0.5 Hz at a force of 20 N. Reproduced from ref. 135 with permission from Springer Nature, copyright 2020.

employed as both the electrode material and piezoelectric nanofiller to fabricate a self-charging supercapacitor based on the PVDF-siloxene piezo-separator. As previously revealed in PVDF composite piezoelectric films, the incorporation of 2D materials fillers led to improved mechanical energy-harvesting properties of PVDF. The PVDF-siloxene piezo-film provided an enhanced output feature ($V_{oc} = \sim 6.5$ V) compared to bare PVDF ($V_{oc} = \sim 3$ V), due to the enhanced dipole alignments in PVDF after the incorporation of siloxene sheets (Fig. 10I and J).[135] The self-charging ability of the siloxene-PVDF supercapacitor was 207 mV, 102 mV and 59 mV within 250 s under a compressive force of 20 N at 2, 1 and 0.5 Hz, respectively. The corresponding self-charging capacitance of the siloxene SC supercapacitor was ~ 3.62 mF cm^{-2}.

Piezoelectric biopolymers provide an alternative choice for piezo-separators, in addition to PVDF. They offer the merits of biodegradability, non-toxicity and biocompatibility.[157] The piezoelectricity of collagen fibrils relies on the hydrogen bonds linked to polypeptides.[158] Maitra *et al.* designed and fabricated an environmentally friendly, portable, wearable and self-charging solid-state supercapacitor, which incorporated a bio-piezoelectric fish swim bladder as the separator (Fig. 11A).[136]

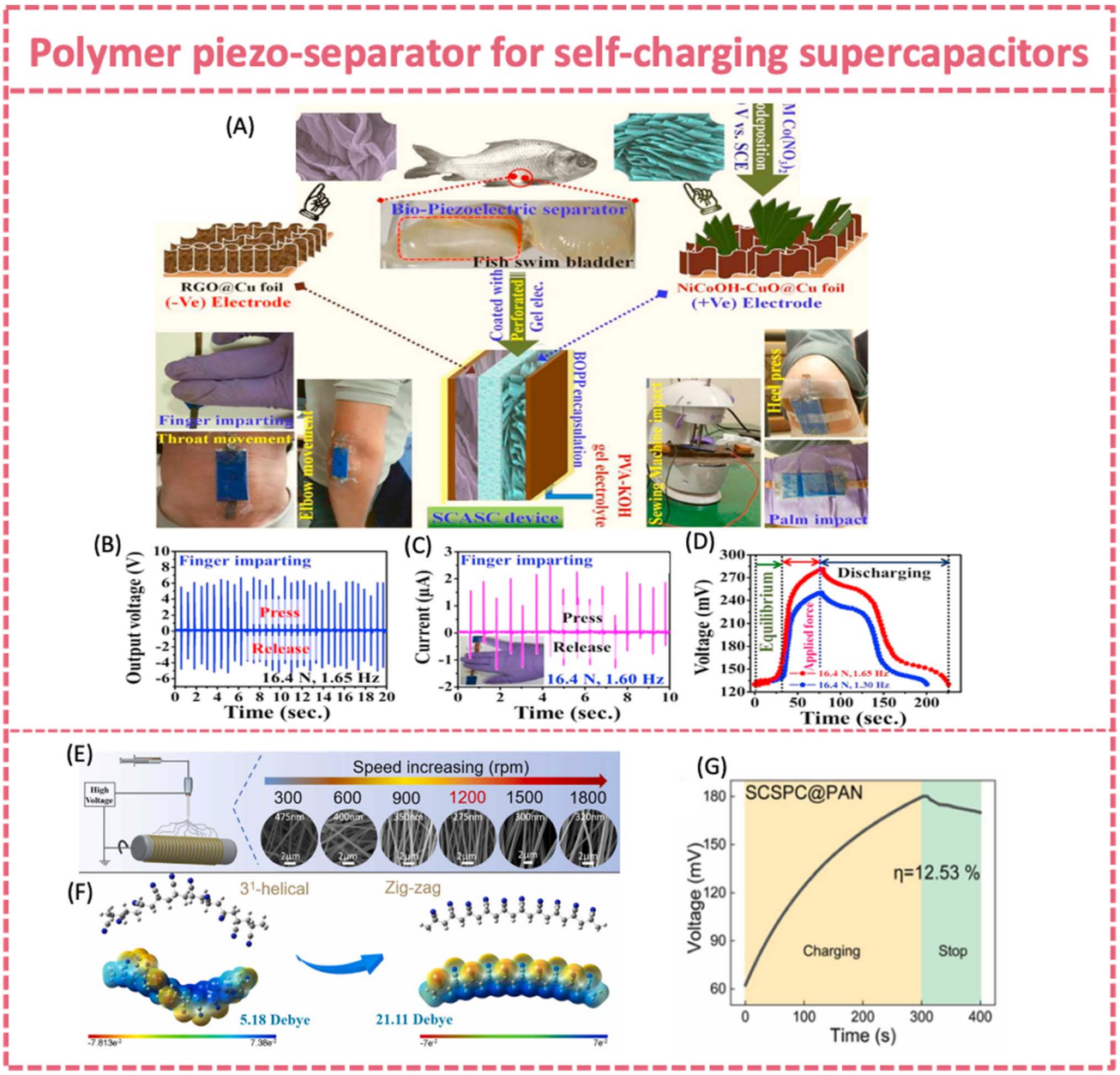

Fig. 11 (A) Fabrication techniques of the SCASC device made of NiCoOH-CuO@Cu foil (positive) and RGO@Cu foil (negative) electrodes separated using a fish swim bladder. (B) Output voltage and (C) short circuit current response of the nanogenerator upon repeated finger imparting. (D) Self-charging and discharging process under human finger imparting. Reproduced from ref. 136 with permission from Elsevier, copyright 2017. (E) Morphology and fiber diameter of PAN nanofibers and (F) density functional theory (DFT) simulations at different roller speeds. (G) The self-charging behavior of SCSPC@PAN under a force of 30 N and at a frequency of 1.5 Hz. Reproduced from ref. 138 with permission from Elsevier, copyright 2023.

The piezoelectric effect of the fish bladder relied on the deformation of the collagen's helical structure and consequent generation of dipole moments under repeated compressive stress. The bio-nanogenerator achieved an average voltage of ~6.23 V and a current of ~1.74 μA upon an applied force of ~16.4 N at 1.65 Hz. The self-charging behavior of the flexible supercapacitor with the fish bladder and PVA-KOH gel electrolyte was studied under finger pressing at 16.4 N and 1.65 Hz (Fig. 11B–D). It was charged from an initial voltage of ~130.1 mV to 281.3 mV after ~80 s of finger motion. Later on, a bio-waste fish scale was also explored as a bio-piezoelectric separator to construct a self-charging supercapacitor.[137] The fish scale nanogenerator provided an open circuit voltage of ~3.6 V. The self-charging device consisted of a MnO_2 positive electrode, an Fe–Mn sulfide@reduced graphene oxide negative electrode and the fish scale piezo-separator. It was charged to ~350 mV from ~115 mV within 20 s under finger pressing. The device can be finally charged to ~448 mV upon finger pressing/releasing circles.

Based on the improved piezoelectric output of electrospun PAN nanofibers (2.0 V over an area of 5 cm^2) *via* structure modulation, a multi-scale aligned high-performance PAN piezoelectric separator was prepared. It demonstrated excellent hydrophilicity, high mechanical properties, good thermal stability, and high piezoelectric properties. The ordered alignment of PAN fibers was realized by an appropriate rotation speed during electrospinning. The zig-zag conformation content and the molecular orientation factor reached the maximum value when PAN nanofiber obtained at a rotation speed of 1200 rpm (Fig. 11E).[138] The theoretical simulation revealed that the zig-zag conformation with higher order of –CN has higher dipole moment, leading to improved piezoelectric properties. Consequently, the output voltage and current of PAN nanofibers reached a maximum value of 4.5 V and 2.1 μA (a working area of 4 cm^2 under 30 N at 1.5 Hz). The SCPS using the PAN piezo-separator and activated carbon cloth electrodes demonstrated a self-charged voltage increase of 117.8 mV under 30 N at 1.5 Hz (Fig. 11G). Most importantly, the PAN piezo-separator exhibited much improved electrochemical performance compared to bare PVDF and PVDF composite piezo-separators, with respect to the higher power density and energy density of the device based on the PAN separator. It was presumed that the high orientation of nanofibers and improved hydrophilicity guaranteed excellent electrochemical performance.

4.2 Polymer-based piezoelectric electrolyte for SCPSs

Piezoelectric electrolyte is developed on the basis of polymer solid-state electrolyte or gel polymer electrolyte (GPE). GPE is a quasi solid-state electrolyte with the advantages of both solid-state and liquid electrolytes. It has improved ionic conductivity compared to solid-state electrolyte and better safety than liquid electrolyte. GPE demonstrates a favourable balance between mechanical and electrochemical properties. GPE consists of a polymer matrix with a liquid solvent containing electrolyte salt enveloped in the polymer network. The solvated polymer networks provide high mobility to enable free ion migration.

Selection criteria for polymer hosts include active chain segment motion, promoted salt dissociation, low glass transition temperature and a wide electrochemical window.[159] The electrolyte salts are expected to have large anions with low dissociation energy to provide charge carriers.[160] The ideal solvent for GPE should have a high dielectric constant, non-volatility, a large donor number and low viscosity.[161,162] Commonly used solvents include water, ethylene carbonate (EC), propylene carbonate (PC), *etc.* The liquid electrolyte can also be an acid solution for GPE used in supercapacitors, such as H_2SO_4/H_2O and H_3PO_4/H_2O.

For supercapacitor application, PVA-based GPEs are most extensively studied. As a water-soluble, mass-produced synthetic resin, PVA has many fascinating features including high flexibility, easy processability, chemical stability and environmental friendliness. The abundant hydroxyl groups in PVA are beneficial for aqueous electrolyte uptake thereby enhancing ionic conductivity. Various kinds of PVA-based GPE have been developed for use in supercapacitors under a wide range of conditions, such as PVA/H_2SO_4,[163] PVA/KOH,[164] PVA/H_3PO_4,[165] PVA/KCl,[166] and PVA/Na_2SO_4.[167] For batteries (take lithium-ion batteries as an example), PVDF and its copolymers are the popular choice as the polymer matrix for GPE. The high dielectric permittivity of PVDF enhances ion dissociation, thereby ensuring good electrochemical performance.[59] The favorable wettability of PVDF with liquid electrolytes, coupled with its high mechanical strength, renders it well-suited as a scaffold material.

The electrochemical performance of PVDF-based gel polymer electrolytes (GPEs) can be further enhanced through the incorporation of other polymers or inorganic fillers, which can be achieved by modulating crystallinity and providing additional ion binding sites.[168] Similarly, further enhancement of PVA-based GPEs can be achieved through the incorporation of inorganic materials or nanosheets. The impact of these added materials on ionic conductivity is closely tied to their specific surface area and surface chemistry.[162] The strategies mentioned above for composite electrolytes also hold significant reference value for incorporating inorganic fillers into polymers to enhance piezoelectric properties.

4.2.1 Polymer based piezo-electrolyte for self-charging batteries. Replacing conventional separators with piezoelectric films offers a straightforward route to fabricate all-in-one SCPSs. The use of piezoelectric polymer solid-state electrolyte is more intriguing as it eliminates the need for an additional separator. This type of polymer solid-state "piezo-electrolyte" merges the functions of piezoelectric film separators and polymer solid-state electrolyte, endowing the assembled SCPS with high flexibility and ease of assembly. For metal ion batteries, the commonly used matrix for polymer electrolyte, PVDF, is a natural choice to obtain piezo-electrolyte due to its intrinsic piezoelectricity. Following the strategy used in piezo-films for PENGs, piezo-ceramic fillers can be integrated into PVDF to enhance the piezoelectric output. A piezo-electrolyte was facilely realized *via* immobilizing liquid $LiPF_6$ electrolyte in a mesoporous PVDF film (Fig. 12A).[134] The battery-type SCPS with a $LiCoO_2$ cathode, a graphite anode and PVDF-$LiPF_6$ piezo-electrolyte sealed in a stainless-steel case could be charged by compressive deformation and stored a 0.118 μAh capacity within 240 s, which surpassed a non-integrated designed self-charging battery by 5 times. Such an SCPS with flexible design could be charged by either periodic compressive force (30 N, 1 Hz) or finger-bending deformation at a frequency of 1 Hz. For the latter configuration, the device was charged from 100 to 184 mV within 5 min and maintained similar electrochemical performance after bending 20 times (Fig. 12C and D). A flexible self-charging sodium-ion battery was constructed, using $BaTiO_3$-P(VDF-HFP)-$NaClO_4$ piezoelectric gel-electrolyte, an $Na_3V_2(PO_4)_3$ (NVP)/@C cathode and a hard carbon anode (Fig. 12E).[139] BTO particles were first incorporated into P(VDF-HFP) to form a composite film with enhanced piezoelectric properties. The piezoelectric gel-electrolyte was formed by immersing the pre-poled film into $NaClO_4$ liquid electrolyte. The assembled flexible device was self-charged from 80 to 320 mV by repeated bending for 300 s in the initial stage and

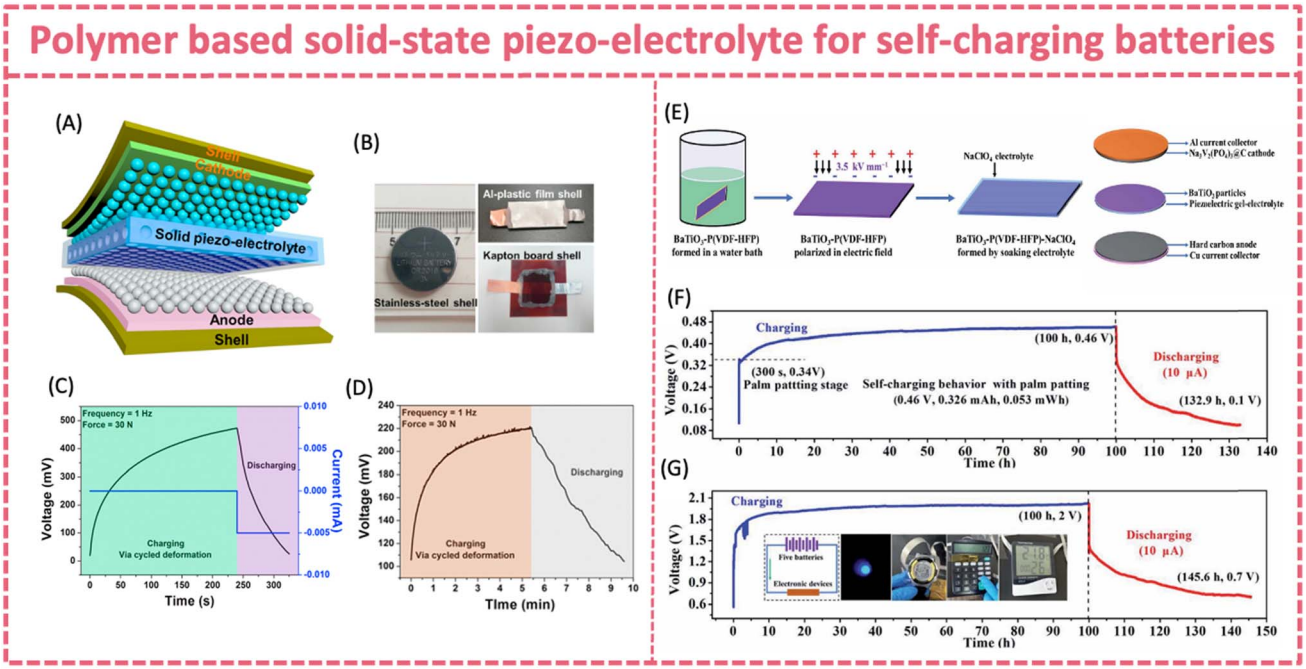

Fig. 12 (A) Design of an all-solid-state SCPC made of graphite (anode) and $LiCoO_2$ (cathode) separated using PVDF-$LiPF_6$ solid piezo-electrolyte. (B) Optical images of the all-solid state SCPC. (C) Self-charging process of an all-solid-state SCPC (sealed in a stainless-steel cell) and (D) flexible SCPC under periodic applied force. Reproduced from ref. 134 with permission from Elsevier, copyright 2017. (E) Fabrication process of a flexible SCSFB made of $Na_3V_2(PO_4)_3$@C (cathode) and hard carbon (anode) separated using $BaTiO_3$-P(VDF-HFP)-$NaClO_4$ piezoelectric gel-electrolyte. (F) Self-charging behavior of a single device and (G) connected devices. Reproduced from ref. 139 with permission from the Royal Society of Chemistry, copyright 2020.

experienced a further voltage increase up to 400 mV in the following 100 h even after the bending was removed. Similar self-charging behavior was also demonstrated when using palm patting mode, which exhibited a 230 mV voltage increase within 300 s. The device stored over 0.3 mA h energy for either bending or patting modes (Fig. 12F, GA). Five serially connected flexible SCPSs could be self-charged to 2.0 V by palm patting, successfully powering a blue LED lamp, a smart watch, an electric calculator or a humidity indicator in a good working state.

4.2.2 Polymer-based piezo-electrolyte for self-charging supercapacitors. PVA based gel-type electrolytes have been extensively applied in flexible supercapacitors to achieve both mechanical flexibility and good electrochemical performance.[162] Therefore, one of the most straightforward methods for creating flexible piezo-electrolyte is to combine piezoelectric materials with PVA gel-electrolyte, following the strategies applied in composite piezoelectric films with non-piezoelectric polymers. Zhou *et al.* developed PVA/KOH/$BaTiO_3$ to fabricate a self-charging flexible solid-state supercapacitor using $NiCo_2O_4$@activated carbon cloth electrodes (Fig. 13A).[142] The flexible device could be easily charged from 0.035 V to 0.12 V by repeated bending at 60° at 1.5 Hz. The self-charging voltage raised to 0.2 V and 0.25 V at a large bending angle of 90° and 180°, respectively (Fig. 13B). Combined with PVA/H_3PO_4 gel-electrolyte with potassium sodium niobate (KNN), a stretchable self-charging supercapacitor (SCSC) with a high biaxial stretchability of 300% was designed (Fig. 13C).[140] The stretchable SCSC could simultaneously harvest and store mechanical energy *via* stretchable piezoelectric gel-electrolyte without a rectifier. When repeatedly stretched by hands for ~40 s (1 Hz), a single stretchable device experienced a voltage increase from 0.01 to 0.12 V in the initial stage, which then further increased to 0.8 V after the stretching terminated. A maximum value of about 1.0 V (from 0.13 V) was finally reached after 300 s of palm patting at 2 Hz and then stopped (Fig. 13D and E). A PVA-KCl-$BaTiO_3$ piezo-electrolyte was prepared by blending BTO particles into PVA-KCl gel electrolyte (Fig. 13F).[141] Coupled with Co-doped Fe_2O_3 anchored activated carbon cloth electrodes, the assembled flexible supercapacitor could work over 1.2 V with an areal capacitance of ~2.86 mF cm^{-2}. It could be easily self-charged to approximately 120 mV by repeated bending for 7 min at a frequency of 1.0 Hz, demonstrating practical potential when connected in series (Fig. 13G). A piezo-powered supercapacitor (PPSC) device was fabricated using iron-doped graphitic carbon nitride (Fe_2O_3-g-C_3N_4) electrodes and a multifunctional nanogenerator/solid-state piezo-electrolyte PVA/KOH/carbon-doped zinc stannate (CZTO).[151] It exhibited a self-charging voltage (SCV) of 669.2 mV under finger pressing (9.47 N, 3.7 Hz) for 180 seconds. Interestingly, this device demonstrated real-time piezo-induced SCV-controlled enhanced electromagnetic shielding up to 59.2 dB at 500 mV and 14.5 GHz. Additionally, it showed a unique functional transformation from an electromagnetic radiation reflector into an absorber at an SCV of approximately 90 mV.

Despite PVA based gel-type piezo-electrolytes providing a simple and effective solution for flexible SCSCs, solid-state

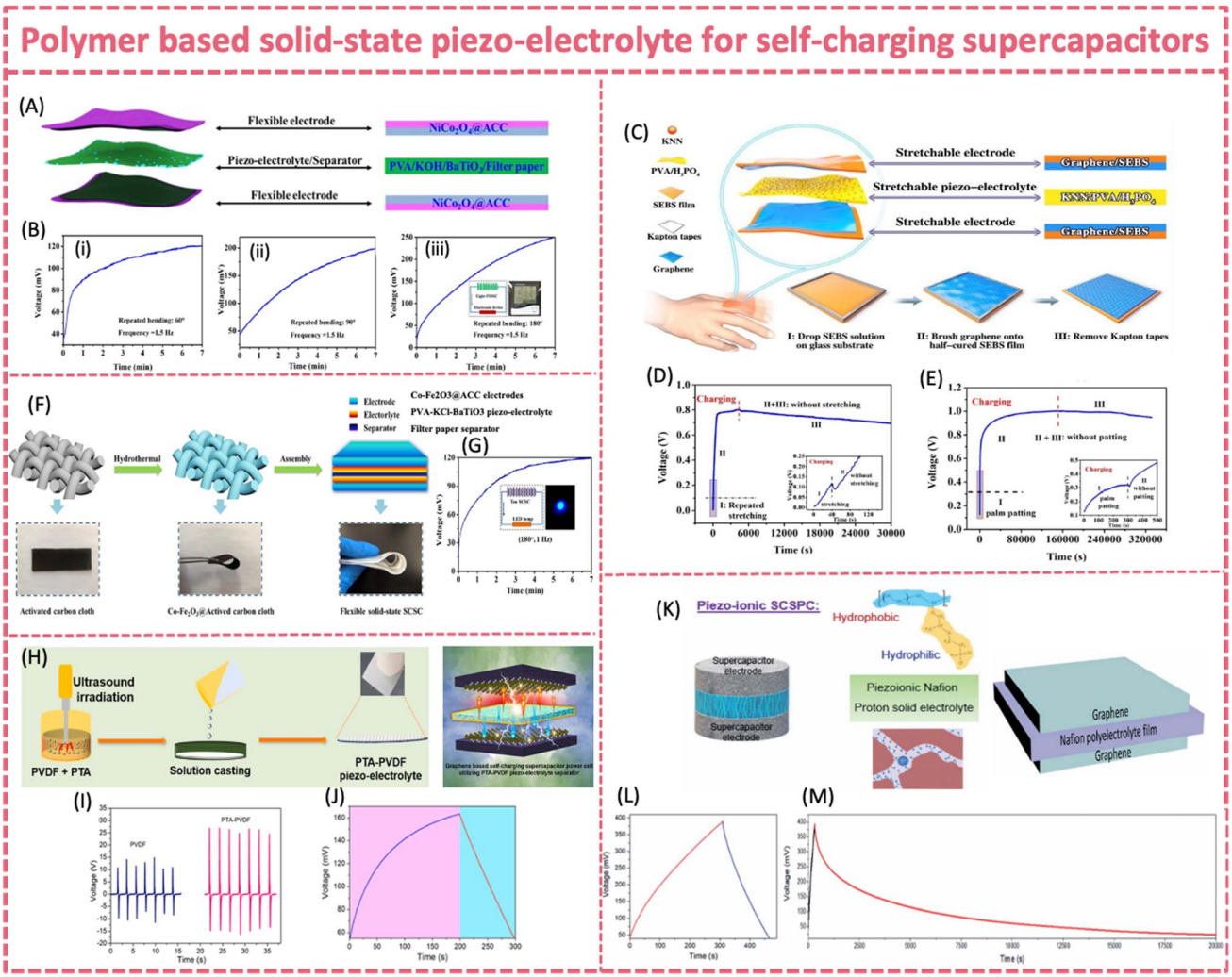

Fig. 13 (A) Structure of an FSSSC made of two $NiCo_2O_4$@ACC electrodes, a PVA/KOH/$BaTiO_3$ piezoelectrolyte, and a filter paper separator. (B) Self-charging behavior at (i) 60°, (ii) 90°, and (iii) 180° repeated bending. Reproduced from ref. 142 with permission from American Chemical Society, copyright 2020. (C) Structure of a stretchable SCSC consisting of graphene/SEBS electrodes and KNN/PVA/H_3PO_4 piezo-electrolyte. (D) Self-charging process of a single device under repeated stretching for about 40 s. (E) Four serially connected devices under palm patting for 300 s. Reproduced from ref. 140 with permission from the Royal Society of Chemistry, copyright 2020. (F) Synthesis and corresponding photographs of the Co-Fe_2O_3@ACC electrode and architecture of the flexible solid-state SCSC. (G) Self-charging curves at 180° repeated bending. Reproduced from ref. 141 with permission from Elsevier, copyright 2021. (H) Preparation of PTA-PVDF piezo-polymer-electrolyte for use in SCSPCs. (I) Current and voltage outputs of the PTA-PVDF film. (J) Self-charging performance of a graphene SCSPC subjected to a compressive force of 2 N. Reproduced from ref. 143 with permission from Elsevier, copyright 2021. (K) Structure of a piezo-ionic SCSPC and molecular structure of Nafion and the ionomeric cavity present in Nafion. (L) Self-charging properties of graphene PI-SCSPC recorded at 10 m s^{-2} and (M) self-discharge profiles of graphene PI-SCSPC monitored over 20 000 seconds. Reproduced from ref. 55 with permission from the Royal Society of Chemistry, copyright 2022.

PVDF based piezo-electrolytes are more attractive due to their high mechanical robustness. Unlike PVA, the PVDF matrix has intrinsic piezoelectricity. Therefore, PVDF-based flexible piezo-electrolyte has the potential to achieve an enhanced mechanical-to-electrochemical conversion efficiency. It should be noted that most of the PVDF based piezo-electrolytes for self-charging supercapacitors follow the piezo-ionic mechanism rather than the piezoelectrochemical process. A piezo-electrolyte film prepared by combining phosphotungstic acid (PTA) and PVDF was developed (Fig. 13H).[143] The addition of solid proton conducting PTA significantly improved the mechanical-to-electrical energy transduction properties, generating a two-fold higher output energy (41 V) than bare PVDF at 1 N force (Fig. 13I and J). The improved energy harvesting properties were attributed to mechano-ionic properties of the PTA-PVDF interface and interfacial polarization due to the Maxwell Wagner Sillars effect.[169,170] Under a compressive force of 2N, the graphene/PTA-PVDF/graphene supercapacitor was charged from 52 to 162 mV within 200 s.

Recent studies revealed that Nafion membranes had exceptional mechano-ionic and piezo-ionic properties and possibly intrinsic piezoelectricity, making them materials of interest in piezo-driven SCPSs.[171–173] Nafion or PVDF-Nafion composites have already demonstrated a strong ability to generate voltage

output under mechanical deformation *via* the piezo/mechano-ionic effect and therefore can be directly used as electrolyte and meanwhile as separators for SCPSs.[171–173] The Nafion membrane generated an output voltage of 910 mV and a short circuit piezo-current of 28 nA at an acceleration of 10 m s^{-2} (Fig. 13K).[55] A flexible solid state MoS_2-Nafion-MoS_2 SCSPC could self-charge up to 294 mV when subjected to an applied force with an acceleration of 10 m s^{-2} in 600 s, which was superior to that of many of the reported SCSPCs. The device was slowly discharged over a time of 13 000 s with a potential decrease of 130 mV, exhibiting excellent charge-retention capability (Fig. 13L and M).

5. Challenges and perspectives

In the past five years, research on self-charging power systems (SCPSs) has undergone rapid development. It was no longer regarded as a sub-topic or peripheral study of PENGs or flexible energy storage devices but rather as a novel and independent research field. The SCPS is a promising energy source for wearable devices with low energy consumption and frequent mechanical deformations, such as wireless health monitors, motion sensors, e-skin and soft robotics. Despite the energy generated by piezo-driven self-charging being small, the cumulative process can provide compensation to extend the battery life of the device. In this review, we provide an overview of the design and mechanism of SCPSs and summarize the recent advances related to polymer or polymer composite piezoelectric separators/electrolyte. Our aim is to draw researchers' attention to address existing problems and drive forward their development for practical implementation. Many issues need to be addressed and key aspects require attention as listed below:

(1) Standard performance metrics. The evaluation of the output index of polymer piezoelectric films, in the form of PENGs, is quite mature and has standard performance metrics. However, the output of a piezo-film in PENGs cannot fully reflect its self-charging capability in SCPSs. One of the most commonly used parameters is the voltage recharged upon the application of forces at a certain frequency. Admittedly, this value may also be strongly affected by many other factors such as the types of electrodes and electrolytes, as well as the dimensions of devices. Thus, it is highly demanded to establish comprehensive, standardized metrics to evaluate the self-charging performance of polymer piezoelectric components.

(2) Flexibility and mechanical durability. While there's no mandatory restriction on the design of the SCPS, it is crucial to prioritize excellent flexibility of the device, especially considering its primary application in wearable and implantable devices. Therefore, flexibility and durability during repeated bending or stretching are required for polymer or polymer composite films. The electrochemical and piezoelectric performances of piezoelectric polymer films upon repeatedly pressing/releasing or mechanical deformation should be emphasized.

(3) Electrochemical performance. Most research on polymer piezo-separator and piezo-electrolyte has focused on the piezoelectric output under applied stress, neglecting their role as components of an energy storage device. It has been noticed that many flexible self-charging supercapacitors using PVDF based piezo-separators exhibited poor capacitive performance especially at high current densities. Future studies should focus on factors affecting electrochemical performance, such as porosity and permeability for piezo-separators and ionic conductivity and electrochemical windows for piezo-electrolytes, and consider them crucial metrics for performance evaluation. For instance, achieving a balance between piezoelectricity and ionic conductivity often involves using inorganic fillers such as 2D materials. These fillers can enhance piezoelectric output and ionic conductivity simultaneously. It is crucial to evaluate how these fillers affect the electrochemical performance of the polymer composite piezoelectric component.

(4) Energy conversion efficiency. Generally speaking, current state-of-the-art self-charging energy storage devices still exhibit very limited self-charging performance with low mechanical-electrochemical energy conversion efficiency. The energy harvested *via* the piezoelectric effect is far from adequate to compensate for the consumption, even for self-charging supercapacitors with relatively low specific energy density.

The challenge in this self-charging power system lies in significantly enhancing the energy output of polymer based piezoelectric components. It can be achieved through various approaches, such as developing novel materials, optimizing the fabrication process, or employing rational structural design. The piezoelectricity of polymers is predominantly influenced by factors such as the crystalline structure, chain alignment and dipole moment, all of which can be tuned by using appropriate processing techniques. Mechanical stretching primarily enhances the alignment of molecular chains, while thermal annealing increases the crystallinity, consequently improving its piezoelectric properties. By modifying electrospinning parameters, the piezoelectroactive content and dipole orientation of the polymer film can be optimized, leading to enhanced piezoelectric output.

Another straightforward yet effective strategy involves incorporating inorganic fillers with strong piezoelectric effects into the polymer matrix to achieve increased piezoelectric output. For example, 2D materials serve as excellent nanofillers for PVDF based piezo-separators or piezo-electrolyte, enhancing both piezoelectric and electrochemical properties. Additionally, employing rational structural design in polymer or polymer composite films, such as porous or lamellar structures, can improve piezoelectric output by achieving optimal deformation format. Regarding device configuration, integration with other energy harvesting units such as pyroelectric and triboelectric components can further boost the energy conversion efficiency of the device.

(5) Mechanism. Piezo-electrochemical and piezo-ionic mechanisms have been proposed to elucidate the self-charging process, and the corresponding post-mortem analysis has also been performed to verify them. For a deep understanding of the mechanism, molecular-level investigation is needed on ion transport in the piezo-separator/piezo-

electrolyte and interfacial behavior between the piezoelectric film and battery components.

In summary, recent advances in polymer and polymer composite films for piezo-driven self-charging power systems (SCPSs) have been reviewed. The mechanism of the device has been briefly introduced, covering the origin of piezoelectricity, configuration design, and piezo-electrochemical/piezo-ionic processes. As derivative research on piezoelectric nanogenerators, piezo-driven SCPSs and PENGs share commonalities in the selection criteria for key materials. Considering the specific requirement of SCPSs, we have summarized the application of polymer-based materials in PENGs, including PVDF and its composites with ZnO, 2D materials and piezo-ceramics, as well as PAN, PVA or non-piezoelectric polymer composites. These materials have already been used as piezoelectric components in SCPSs or have great potential for such devices. The recently developed SCPSs have demonstrated a considerable self-charging performance in batteries or supercapacitors. Despite significant progress, the realization of practical self-charging performance including adequate energy compensation for the piezo-generator part and satisfactory electrochemical performance for the energy storage part remains a big challenge. Exploring novel materials, designing new composite structures and using new processing techniques will advance the development of polymer-based piezoelectric components to meet practical application requirements. These advancements will promote the development of self-charging energy storage devices for wearable, implantable electronics.

Data availability

No primary research results, software or code have been included and no new data were generated or analysed as part of this review.

Author contributions

Kewei Shu: writing – original draft, supervision, writing – review & editing. Wenjuan Li: writing – original draft, visualization. Qijie Wu: writing – review & editing. Yan Zong: writing – review & editing, resources. Chen Zhao: writing – review & editing. Yi Zhang: investigation. Caiyun Wang: writing – review & editing, conceptualization.

Conflicts of interest

There are no conflicts to declare.

Acknowledgements

This work was supported by the National Natural Science Foundation of China (NSFC No. 22105120), the Shaanxi Province Qin Chuangyuan "Scientist + Engineer" Team Construction Project (2024QCY-KXJ-127), and the Jiangsu Excellent Postdoctoral Program (2022ZB649).

References

1 M. Bariya, H. Y. Y. Nyein and A. Javey, *Nat. Electron.*, 2018, **1**, 160–171.
2 W. Gao, H. Ota, D. Kiriya, K. Takei and A. Javey, *Acc. Chem. Res.*, 2019, **52**, 523–533.
3 S. M. A. Iqbal, I. Mahgoub, E. Du, M. A. Leavitt and W. Asghar, *npj Flexible Electron.*, 2021, **5**, 9.
4 Q. Shi, B. Dong, T. He, Z. Sun, J. Zhu, Z. Zhang and C. Lee, *InfoMat*, 2020, **2**, 1131–1162.
5 X. Wang, X. Lu, B. Liu, D. Chen, Y. Tong and G. Shen, *Adv. Mater.*, 2014, **26**, 4763–4782.
6 W. Liu, M.-S. Song, B. Kong and Y. Cui, *Adv. Mater.*, 2017, **29**, 1603436.
7 H. Wang, A. Jasim and X. Chen, *Appl. Energy*, 2018, **212**, 1083–1094.
8 H. Ryu, H.-J. Yoon and S.-W. Kim, *Adv. Mater.*, 2019, **31**, 1802898.
9 C. Ye, D. Liu, P. Chen, L. N. Y. Cao, X. Li, T. Jiang and Z. L. Wang, *Adv. Mater.*, 2023, **35**, 2209713.
10 A. P. Straub, N. Y. Yip, S. Lin, J. Lee and M. Elimelech, *Nat. Energy*, 2016, **1**, 16090.
11 B. Chen, Y. Yang and Z. L. Wang, *Adv. Energy Mater.*, 2018, **8**, 1702649.
12 Z. Li, Q. Zheng, Z. L. Wang and Z. Li, *Research*, 2020, **2020**, 8710686.
13 M. Lee, J. Bae, J. Lee, C.-S. Lee, S. Hong and Z. L. Wang, *Energy Environ. Sci.*, 2011, **4**, 3359–3363.
14 X. Cheng, X. Xue, Y. Ma, M. Han, W. Zhang, Z. Xu, H. Zhang and H. Zhang, *Nano Energy*, 2016, **22**, 453–460.
15 Y. Su, C. Chen, H. Pan, Y. Yang, G. Chen, X. Zhao, W. Li, Q. Gong, G. Xie, Y. Zhou, S. Zhang, H. Tai, Y. Jiang and J. Chen, *Adv. Funct. Mater.*, 2021, **31**, 2010962.
16 M. Zhu, Z. Yi, B. Yang and C. Lee, *Nano Today*, 2021, **36**, 101016.
17 X. Xue, S. Wang, W. Guo, Y. Zhang and Z. L. Wang, *Nano Lett.*, 2012, **12**, 5048–5054.
18 X. Pu, W. Hu and Z. L. Wang, *Small*, 2018, **14**, 1702817.
19 X. Pu and Z. L. Wang, *Chem. Sci.*, 2021, **12**, 34–49.
20 R. Liu, Z. L. Wang, K. Fukuda and T. Someya, *Nat. Rev. Mater.*, 2022, **7**, 870–886.
21 C. Shao, Y. Zhao and L. Qu, *SusMat*, 2022, **2**, 142–160.
22 K. Krishnamoorthy, P. Pazhamalai, S. Manoharan, N. U. H. Liyakath Ali and S.-J. Kim, *Carbon Energy*, 2022, **4**, 833–855.
23 Z. Yang, S. Zhou, J. Zu and D. Inman, *Joule*, 2018, **2**, 642–697.
24 D. Zhou, L. Xue, L. Wang, N. Wang, W.-M. Lau and X. Cao, *Nano Energy*, 2019, **61**, 435–441.
25 W. Li, X. Xu, C. Liu, M. C. Tekell, J. Ning, J. Guo, J. Zhang and D. Fan, *Adv. Funct. Mater.*, 2017, **27**, 1702738.
26 H. Park, J. W. Kim, S. Y. Hong, G. Lee, H. Lee, C. Song, K. Keum, Y. R. Jeong, S. W. Jin, D. S. Kim and J. S. Ha, *ACS Nano*, 2019, **13**, 10469–10480.
27 B. Singh, B. Padha, S. Verma, S. Satapathi, V. Gupta and S. Arya, *J. Energy Storage*, 2022, **47**, 103547.
28 S. Meng, N. Wang and X. Cao, *Materials*, 2023, **16**, 6916.

29 K. Bicy, A. B. Gueye, D. Rouxel, N. Kalarikkal and S. Thomas, *Surf. Interfaces*, 2022, **31**, 101977.
30 L. Lu, W. Ding, J. Liu and B. Yang, *Nano Energy*, 2020, **78**, 105251.
31 J. Yan, M. Liu, Y. G. Jeong, W. Kang, L. Li, Y. Zhao, N. Deng, B. Cheng and G. Yang, *Nano Energy*, 2019, **56**, 662–692.
32 D. W. Jin, Y. J. Ko, C. W. Ahn, S. Hur, T. K. Lee, D. G. Jeong, M. Lee, C.-Y. Kang and J. H. Jung, *Small*, 2021, **17**, 2007289.
33 D. Ho, *ChemElectroChem*, 2024, **11**, e202300268.
34 P. Dineva, D. Gross, R. Müller and T. Rangelov, in *Dynamic Fracture of Piezoelectric Materials, Solid Mechanics and Its Applications*, Springer, Cham, 2014, ch. 2, vol. 212, pp. 7–32.
35 M. Habib, I. Lantgios and K. Hornbostel, *J. Phys. D: Appl. Phys.*, 2022, **55**, 423002.
36 N. Chodankar, C. Padwal, H. D. Pham, K. K. Ostrikov, S. Jadhav, K. Mahale, P. K. D. V Yarlagadda, Y. S. Huh, Y.-K. Han and D. Dubal, *Nano Energy*, 2021, **90**, 106607.
37 H. Liu, J. Zhong, C. Lee, S.-W. Lee and L. Lin, *Appl. Phys. Rev.*, 2018, **5**, 041306.
38 Y. Qi and M. C. McAlpine, *Energy Environ. Sci.*, 2010, **3**, 1275–1285.
39 J. Palosaari, M. Leinonen, J. Hannu, J. Juuti and H. Jantunen, *J. Electroceram.*, 2012, **28**, 214–219.
40 J. Bae, Y. J. Park, M. Lee, S. N. Cha, Y. J. Choi, C. S. Lee, J. M. Kim and Z. L. Wang, *Adv. Mater.*, 2011, **23**, 3446–3449.
41 G. Zhu, R. Yang, S. Wang and Z. L. Wang, *Nano Lett.*, 2010, **10**, 3151–3155.
42 Y. Hu, Y. Zhang, C. Xu, L. Lin, R. L. Snyder and Z. L. Wang, *Nano Lett.*, 2011, **11**, 2572–2577.
43 S. Wang, Z.-H. Lin, S. Niu, L. Lin, Y. Xie, K. C. Pradel and Z. L. Wang, *ACS Nano*, 2013, **7**, 11263–11271.
44 M. B. Starr, J. Shi and X. Wang, *Angew. Chem., Int. Ed.*, 2012, **51**, 5962–5966.
45 M. B. Starr and X. Wang, *Nano Energy*, 2015, **14**, 296–311.
46 A. Ramadoss, B. Saravanakumar, S. W. Lee, Y.-S. Kim, S. J. Kim and Z. L. Wang, *ACS Nano*, 2015, **9**, 4337–4345.
47 R. Song, H. Jin, X. Li, L. Fei, Y. Zhao, H. Huang, H. Lai-Wa Chan, Y. Wang and Y. Chai, *J. Mater. Chem. A*, 2015, **3**, 14963–14970.
48 D. Zhou, N. Wang, T. Yang, L. Wang, X. Cao and Z. L. Wang, *Mater. Horiz.*, 2020, **7**, 2158–2167.
49 E. K. Boahen, B. Pan, H. Kweon, J. S. Kim, H. Choi, Z. Kong, D. J. Kim, J. Zhu, W. Bin Ying and K. J. Lee, *Nat. Commun.*, 2022, **13**, 7699.
50 K. Chen and D. Ho, *Aggregate*, 2024, **5**, e425.
51 W. Takashima, K. Hayasi and K. Kaneto, *Electrochem. Commun.*, 2007, **9**, 2056–2061.
52 P. G. De Gennes, K. Okumura, M. Shahinpoor and K. J. Kim, *Europhys. Lett.*, 2000, **50**, 513.
53 A. Fiumefreddo and M. Utz, *Macromolecules*, 2010, **43**, 5814–5819.
54 Y. Dobashi, D. Yao, Y. Petel, T. N. Nguyen, M. S. Sarwar, Y. Thabet, C. L. W. Ng, E. Scabeni Glitz, G. T. M. Nguyen and C. Plesse, *Science*, 2022, **376**, 502–507.
55 K. Krishnamoorthy, S. Manoharan, V. K. Mariappan, P. Pazhamalai and S.-J. Kim, *J. Mater. Chem. A*, 2022, **10**, 7818–7829.
56 A. Katsaounis, S. Balomenou, D. Tsiplakides, S. Brosda, S. Neophytides and C. G. Vayenas, *Appl. Catal., B*, 2005, **56**, 251–258.
57 J. Nunes-Pereira, C. M. Costa and S. Lanceros-Mendez, *J. Power Sources*, 2015, **281**, 378–398.
58 G. Kang and Y. Cao, *J. Membr. Sci.*, 2014, **463**, 145–165.
59 Y. Wu, Y. Li, Y. Wang, Q. Liu, Q. Chen and M. Chen, *J. Energy Chem.*, 2022, **64**, 62–84.
60 B. Mohammadi, A. A. Yousefi and S. M. Bellah, *Polym. Test.*, 2007, **26**, 42–50.
61 Z. Pi, J. Zhang, C. Wen, Z. Zhang and D. Wu, *Nano Energy*, 2014, **7**, 33–41.
62 A. Salimi and A. A. Yousefi, *Polym. Test.*, 2003, **22**, 699–704.
63 A. Lund, C. Gustafsson, H. Bertilsson and R. W. Rychwalski, *Compos. Sci. Technol.*, 2011, **71**, 222–229.
64 H. Pan, B. Na, R. Lv, C. Li, J. Zhu and Z. Yu, *J. Polym. Sci., Part B: Polym. Phys.*, 2012, **50**, 1433–1437.
65 K. S. Ramadan, D. Sameoto and S. Evoy, *Smart Mater. Struct.*, 2014, **23**, 33001.
66 L. Zhang, J. Gui, Z. Wu, R. Li, Y. Wang, Z. Gong, X. Zhao, C. Sun and S. Guo, *Nano Energy*, 2019, **65**, 103924.
67 R. K. Singh, S. W. Lye and J. Miao, *Sens. Actuators, A*, 2020, **303**, 111841.
68 S. Cha, S. M. Kim, H. Kim, J. Ku, J. I. Sohn, Y. J. Park, B. G. Song, M. H. Jung, E. K. Lee and B. L. Choi, *Nano Lett.*, 2011, **11**, 5142–5147.
69 K. Maity, S. Garain, K. Henkel, D. Schmeißer and D. Mandal, *ACS Appl. Polym. Mater.*, 2020, **2**, 862–878.
70 B. Chu, X. Zhou, K. Ren, B. Neese, M. Lin, Q. Wang, F. Bauer and Qm. Zhang, *Science*, 2006, **313**, 334–336.
71 S. Ma, T. Ye, T. Zhang, Z. Wang, K. Li, M. Chen, J. Zhang, Z. Wang, S. Ramakrishna and L. Wei, *Adv. Mater. Technol.*, 2018, **3**, 1800033.
72 C. M. Costa, V. F. Cardoso, P. Martins, D. M. Correia, R. Goncalves, P. Costa, V. Correia, C. Ribeiro, M. M. Fernandes, P. M. Martins and S. Lanceros-Mendez, *Chem. Rev.*, 2023, **123**, 11392–11487.
73 A. Gebrekrstos, T. S. Muzata and S. S. Ray, *ACS Appl. Nano Mater.*, 2022, **5**, 7632–7651.
74 S. Rana, V. Singh and B. Singh, *iScience*, 2022, **25**, 103748.
75 J. Zhou, D. Hou, S. Cheng, J. Zhang, W. Chen, L. Zhou and P. Zhang, *Mater. Today Energy*, 2023, **31**, 101208.
76 A. Anand and M. C. Bhatnagar, *Mater. Today Energy*, 2019, **13**, 293–301.
77 N. Chamankar, R. Khajavi, A. A. Yousefi, A. Rashidi and F. Golestanifard, *Ceram. Int.*, 2020, **46**, 19669–19681.
78 S. Bairagi and S. W. Ali, *Eur. Polym. J.*, 2019, **116**, 554–561.
79 R. Han, L. Zheng, G. Li, G. Chen, S. Ma, S. Cai and Y. Li, *ACS Appl. Mater. Interfaces*, 2021, **13**, 46738–46748.
80 G. Tian, W. Deng, Y. Gao, D. Xiong, C. Yan, X. He, T. Yang, L. Jin, X. Chu, H. Zhang, W. Yan and W. Yang, *Nano Energy*, 2019, **59**, 574–581.
81 A. Patra, A. Pal and S. Sen, *Ceram. Int.*, 2018, **44**, 11196–11203.
82 X. Du, Z. Zhou, Z. Zhang, L. Yao, Q. Zhang and H. Yang, *J. Adv. Ceram.*, 2022, **11**, 331–344.

83 Y. Zhao, Q. Liao, G. Zhang, Z. Zhang, Q. Liang, X. Liao and Y. Zhang, *Nano Energy*, 2015, **11**, 719–727.
84 B. Dudem, D. H. Kim, L. K. Bharat and J. S. Yu, *Appl. Energy*, 2018, **230**, 865–874.
85 X. Hu, X. Yan, L. Gong, F. Wang, Y. Xu, L. Feng, D. Zhang and Y. Jiang, *ACS Appl. Mater. Interfaces*, 2019, **11**, 7379–7386.
86 K. Batra, N. Sinha and B. Kumar, *J. Mater. Sci.: Mater. Electron.*, 2019, **30**, 6157–6165.
87 J. Fu, Y. Hou, M. Zheng and M. Zhu, *ACS Appl. Mater. Interfaces*, 2020, **12**, 9766–9774.
88 B. S. Athira, A. George, K. Vaishna Priya, U. S. Hareesh, E. B. Gowd, K. P. Surendran and A. Chandran, *ACS Appl. Mater. Interfaces*, 2022, **14**, 44239–44250.
89 B. Ponraj, R. Bhimireddi and K. B. R. Varma, *J. Adv. Ceram.*, 2016, **5**, 308–320.
90 Z. L. Wang and J. Song, *Science*, 2006, **312**, 242–246.
91 C.-Y. Chen, G. Zhu, Y. Hu, J.-W. Yu, J. Song, K.-Y. Cheng, L.-H. Peng, L.-J. Chou and Z. L. Wang, *ACS Nano*, 2012, **6**, 5687–5692.
92 Y.-F. Lin, J. Song, Y. Ding, S.-Y. Lu and Z. L. Wang, *Appl. Phys. Lett.*, 2008, **92**, 022105.
93 R. Yang, Y. Qin, L. Dai and Z. L. Wang, *Nat. Nanotechnol.*, 2009, **4**, 34–39.
94 S. Xu, Y. Qin, C. Xu, Y. Wei, R. Yang and Z. L. Wang, *Nat. Nanotechnol.*, 2010, **5**, 366–373.
95 P. Thakur, A. Kool, N. A. Hoque, B. Bagchi, F. Khatun, P. Biswas, D. Brahma, S. Roy, S. Banerjee and S. Das, *Nano Energy*, 2018, **44**, 456–467.
96 K. H. Michel and B. Verberck, *Phys. Rev. B: Condens. Matter Mater. Phys.*, 2011, **83**, 115328.
97 K.-A. N. Duerloo, M. T. Ong and E. J. Reed, *J. Phys. Chem. Lett.*, 2012, **3**, 2871–2876.
98 S. K. Kim, R. Bhatia, T.-H. Kim, D. Seol, J. H. Kim, H. Kim, W. Seung, Y. Kim, Y. H. Lee and S.-W. Kim, *Nano Energy*, 2016, **22**, 483–489.
99 W. Wu, L. Wang, Y. Li, F. Zhang, L. Lin, S. Niu, D. Chenet, X. Zhang, Y. Hao, T. F. Heinz, J. Hone and Z. L. Wang, *Nature*, 2014, **514**, 470–474.
100 R. Hinchet, U. Khan, C. Falconi and S.-W. Kim, *Mater. Today*, 2018, **21**, 611–630.
101 M. N. Blonsky, H. L. Zhuang, A. K. Singh and R. G. Hennig, *ACS Nano*, 2015, **9**, 9885–9891.
102 R. Fei, W. Li, J. Li and L. Yang, *Appl. Phys. Lett.*, 2015, **107**, 173104.
103 Y. Li, Y. Rao, K. F. Mak, Y. You, S. Wang, C. R. Dean and T. F. Heinz, *Nano Lett.*, 2013, **13**, 3329–3333.
104 J. Yang, Y. Zhang, Y. Li, Z. Wang, W. Wang, Q. An and W. Tong, *Mater. Today Commun.*, 2021, **26**, 101629.
105 S. S. Nardekar, K. Krishnamoorthy, P. Pazhamalai, S. Sahoo and S. J. Kim, *Nano Energy*, 2022, **93**, 106869.
106 T. Huang, S. Yang, P. He, J. Sun, S. Zhang, D. Li, Y. Meng, J. Zhou, H. Tang and J. Liang, *ACS Appl. Mater. Interfaces*, 2018, **10**, 30732–30740.
107 H. Li, W. Zhang, Q. Ding, X. Jin, Q. Ke, Z. Li, D. Wang and C. Huang, *ACS Appl. Mater. Interfaces*, 2019, **11**, 38023–38030.
108 T. H. Cho, T. Sakai, S. Tanase, K. Kimura, Y. Kondo, T. Tarao and M. Tanaka, *Electrochem. Solid-State Lett.*, 2007, **10**, A159–A162.
109 T.-H. Cho, M. Tanaka, H. Ohnishi, Y. Kondo, M. Yoshikazu, T. Nakamura and T. Sakai, *J. Power Sources*, 2010, **195**, 4272–4277.
110 J. Tao, Y. Wang, X. Zheng, C. Zhao, X. Jin, W. Wang and T. Lin, *Nano Energy*, 2023, **118**, 108987.
111 Z.-Y. Wang, K.-H. Su, H.-Q. Fan and Z.-Y. Wen, *Polymer*, 2008, **49**, 2542–2547.
112 L. Persano, A. Camposeo, C. Tekmen and D. Pisignano, *Macromol. Mater. Eng.*, 2013, **298**, 504–520.
113 W. Wang, Y. Zheng, X. Jin, Y. Sun, B. Lu, H. Wang, J. Fang, H. Shao and T. Lin, *Nano Energy*, 2019, **56**, 588–594.
114 R. M. Street, M. Minagawa, A. Vengrenyuk and C. L. Schauer, *J. Appl. Polym. Sci.*, 2019, **136**, 47530.
115 S. Yu, J. Milam-Guerrero, Y. Tai, S. Yang, Y. Y. Choi, J. Nam and N. V Myung, *ACS Appl. Polym. Mater.*, 2021, **4**, 635–644.
116 T. Cai, Y. Yang, T. Bi, E. Bi and Y. Li, *Nanotechnology*, 2020, **31**, 24LT01.
117 L. Yuan, W. Fan, X. Yang, S. Ge, C. Xia, S. Y. Foong, R. K. Liew, S. Wang, Q. Van Le and S. S. Lam, *Compos. Commun.*, 2021, **25**, 100680.
118 S. Bairagi, A. Chowdhury, S. Banerjee, A. Thakre, A. Saini and S. W. Ali, *J. Mater. Sci.: Mater. Electron.*, 2022, **33**, 13152–13165.
119 L. E. Greene, M. Law, J. Goldberger, F. Kim, J. C. Johnson, Y. Zhang, R. J. Saykally and P. Yang, *Angew. Chem., Int. Ed.*, 2003, **42**, 3031–3034.
120 L. E. Greene, M. Law, D. H. Tan, M. Montano, J. Goldberger, G. Somorjai and P. Yang, *Nano Lett.*, 2005, **5**, 1231–1236.
121 Y. P. Lim, J. S. C. Koay, J. Zhao, S. Huang, B. T. Goh, K. C. Aw, B. Chen, C. Y. Haw and W. C. Gan, *Adv. Funct. Mater.*, 2022, **32**, 2206750.
122 M. Manikandan, P. Rajagopalan, N. Patra, S. Jayachandran, M. Muralidharan, S. S. M. Prabu, I. A. Palani and V. Singh, *Nanotechnology*, 2020, **31**, 185401.
123 Y. Guan, M. Bai, Q. Wang, L. Liu, S. Yu, B. Kong, F. Lv, M. Guo, G. Liu, L. Li, L. Zhang, Y. Lin and W. Li, *Chem. Eng. J.*, 2023, **460**, 141598.
124 X. Chen, K. Parida, J. Wang, J. Xiong, M.-F. Lin, J. Shao and P. S. Lee, *ACS Appl. Mater. Interfaces*, 2017, **9**, 42200–42209.
125 C. K. Jeong, J. H. Han, H. Palneedi, H. Park, G.-T. Hwang, B. Joung, S.-G. Kim, H. J. Shin, I.-S. Kang and J. Ryu, *APL Mater.*, 2017, **5**, 074102.
126 M.-H. Zhang, Q. Zhang, T.-T. Yu, G. Li, H.-C. Thong, L.-Y. Peng, L. Liu, J. Ma, Y. Shen, Z. Shen, J. Daniels, L. Gu, B. Han, L.-Q. Chen, J.-F. Li, F. Li and K. Wang, *Mater. Today*, 2021, **46**, 44–53.
127 Y.-Y.-S. Cheng, L. Liu, Y. Huang, L. Shu, Y.-X. Liu, L. Wei and J.-F. Li, *ACS Appl. Mater. Interfaces*, 2021, **13**, 39633–39640.
128 S. Yu, Y. Ling, S. Sun, Y. Wang, Z. Yu, J. Zheng, G. Liu, D. Chen, Y. Fu, Y. Liu and H. Zhou, *Nano Energy*, 2022, **94**, 106911.
129 X. Xue, P. Deng, B. He, Y. Nie, L. Xing, Y. Zhang and Z. L. Wang, *Adv. Energy Mater.*, 2014, **4**, 1301329.

130 Y. Zhang, Y. Zhang, X. Xue, C. Cui, B. He, Y. Nie, P. Deng and Z. Lin Wang, *Nanotechnology*, 2014, **25**, 105401.
131 A. Rasheed, W. He, Y. Qian, H. Park and D. J. Kang, *ACS Appl. Mater. Interfaces*, 2020, **12**, 20891–20900.
132 K. Parida, V. Bhavanasi, V. Kumar, J. Wang and P. S. Lee, *J. Power Sources*, 2017, **342**, 70–78.
133 X. Gao, Y. Zhang, Y. Zhao, S. Yin, J. Gui, C. Sun and S. Guo, *Nano Energy*, 2022, **91**, 106701.
134 H. He, Y. Fu, T. Zhao, X. Gao, L. Xing, Y. Zhang and X. Xue, *Nano Energy*, 2017, **39**, 590–600.
135 K. Krishnamoorthy, P. Pazhamalai, V. K. Mariappan, S. S. Nardekar, S. Sahoo and S. J. Kim, *Nat. Commun.*, 2020, **11**, 1–11.
136 A. Maitra, S. K. Karan, S. Paria, A. K. Das, R. Bera, L. Halder, S. K. Si, A. Bera and B. B. Khatua, *Nano Energy*, 2017, **40**, 633–645.
137 A. Paul, A. Chakraborty, P. Samanta, D. Mondal, D. Dhak, N. C. Murmu and T. Kuila, *J. Energy Storage*, 2023, **74**, 109426.
138 C. Zhao, J. Xu, J. Tao, C. Xiao, X. Jin, W. Wang, X. Liu, J. Chen and Z. Zhu, *Nano Energy*, 2023, **116**, 108812.
139 D. Zhou, T. Yang, J. Yang and L. Fan, *J. Mater. Chem. A*, 2020, **8**, 13267–13276.
140 D. Zhou, N. Wang, T. Yang, L. Wang, X. Cao and Z. L. Wang, *Mater. Horiz.*, 2020, **7**, 2158–2167.
141 D. Zhou, F. Wang, J. Yang and L. Fan, *Chem. Eng. J.*, 2021, **406**, 126825.
142 D. Zhou, F. Wang, X. Zhao, J. Yang, H. Lu, L.-Y. Lin and L.-Z. Fan, *ACS Appl. Mater. Interfaces*, 2020, **12**, 44883–44891.
143 S. Manoharan, P. Pazhamalai, V. K. Mariappan, K. Murugesan, S. Subramanian, K. Krishnamoorthy and S.-J. Kim, *Nano Energy*, 2021, **83**, 105753.
144 P. Pazhamalai, K. Krishnamoorthy, V. K. Mariappan, S. Sahoo, S. Manoharan and S. J. Kim, *Adv. Mater. Interfaces*, 2018, **5**, 1–9.
145 Y. Lu, Y. Jiang, Z. Lou, R. Shi, D. Chen and G. Shen, *Prog. Nat. Sci.: Mater. Int.*, 2020, **30**, 174–179.
146 A. De Adhikari, S. Singh and I. Lahiri, *J. Alloys Compd.*, 2023, **939**, 168713.
147 Y.-S. Kim, Y. Xie, X. Wen, S. Wang, S. J. Kim, H.-K. Song and Z. L. Wang, *Nano Energy*, 2015, **14**, 77–86.
148 S. Jadhav, H. D. Pham, C. Padwal, M. Chougale, C. Brown, N. Motta, K. (Ken) Ostrikov, J. Bae and D. Dubal, *Adv. Mater. Technol.*, 2022, **7**, 2100550.
149 P. Pazhamalai, V. K. Mariappan, S. Sahoo, W. Y. Kim, Y. S. Mok and S.-J. Kim, *Micromachines*, 2020, **11**, 198.
150 R. Liu, H. Chen, B. Zhang, Z. Liu, Y. Fan, L.-Z. Fan and D. Zhou, *Chem. Eng. J.*, 2024, **484**, 149513.
151 P. P. Singh and B. B. Khatua, *ACS Appl. Mater. Interfaces*, 2024, **16**, 11050–11061.
152 V. Deimede and C. Elmasides, *Energy Technol.*, 2015, **3**, 453–468.
153 C. M. Costa, Y.-H. Lee, J.-H. Kim, S.-Y. Lee and S. Lanceros-Méndez, *Energy Storage Mater.*, 2019, **22**, 346–375.
154 C. M. Costa and S. Lanceros-Mendez, *Curr. Opin. Electrochem.*, 2021, **29**, 100752.
155 P. Arora and Z. Zhang, *Chem. Rev.*, 2004, **104**, 4419–4462.
156 S. Mishra, L. Unnikrishnan, S. K. Nayak and S. Mohanty, *Macromol. Mater. Eng.*, 2019, **304**, 1800463.
157 R. Wang, J. Sui and X. Wang, *ACS Nano*, 2022, **16**, 17708–17728.
158 S. Bera, S. Guerin, H. Yuan, J. O'Donnell, N. P. Reynolds, O. Maraba, W. Ji, L. J. W. Shimon, P.-A. Cazade, S. A. M. Tofail, D. Thompson, R. Yang and E. Gazit, *Nat. Commun.*, 2021, **12**, 2634.
159 W. H. Meyer, *Adv. Mater.*, 1998, **10**, 439–448.
160 V. Aravindan, J. Gnanaraj, S. Madhavi and H. Liu, *Chem.–Eur. J.*, 2011, **17**, 14326–14346.
161 W. Ren, C. Ding, X. Fu and Y. Huang, *Energy Storage Mater.*, 2021, **34**, 515–535.
162 S. Alipoori, S. Mazinani, S. H. Aboutalebi and F. Sharif, *J. Energy Storage*, 2020, **27**, 101072.
163 K. Shu, C. Wang, S. Li, C. Zhao, Y. Yang, H. Liu and G. Wallace, *J. Mater. Chem. A*, 2015, **3**, 4428–4434.
164 C. Xiong, W. Dang, S. Nie, C. Qin, D. Li, L. Dai, M. Shen, Y. Xu and Y. Ni, *Cellulose*, 2021, **28**, 1455–1468.
165 C. Zhao, C. Wang, Z. Yue, K. Shu and G. G. Wallace, *ACS Appl. Mater. Interfaces*, 2013, **5**, 9008–9014.
166 K. Sun, E. Feng, G. Zhao, H. Peng, G. Wei, Y. Lv and G. Ma, *ACS Sustain. Chem. Eng.*, 2019, **7**, 165–173.
167 L. Zhang, P. Zhu, F. Zhou, W. Zeng, H. Su, G. Li, J. Gao, R. Sun and C. Wong, *ACS Nano*, 2016, **10**, 1273–1282.
168 L. Long, S. Wang, M. Xiao and Y. Meng, *J. Mater. Chem. A*, 2016, **4**, 10038–10069.
169 Y. Dobashi, G. Allegretto, M. S. Sarwar, E. Cretu and J. D. W. Madden, *MRS Adv.*, 2016, **1**, 63–68.
170 J. Yuennan, P. Sukwisute and N. Muensit, *Mater. Res. Express*, 2018, **5**, 55702.
171 Y. Liu, Y. Hu, J. Zhao, G. Wu, X. Tao and W. Chen, *Small*, 2016, **12**, 5074–5080.
172 C. Xu, L. Zhang, Y. Xu, Z. Yin, Q. Chen, S. Ma, H. Zhang, R. Huang, C. Zhang, L. Jin, W. Yang and J. Lu, *J. Mater. Chem. A*, 2017, **5**, 189–200.
173 O. C. Yılmaz, I. Sen, B. O. Gurses, O. Ozdemir, L. Cetin, M. Sarıkanat, Y. Seki, K. Sever and E. Altinkaya, *Composites, Part B*, 2019, **165**, 747–753.